Chemical Engineering Journal 453 (2023) 139541

Contents lists available at ScienceDirect

Chemical Engineering Journal

journal homepage: www.elsevier.com/locate/cej

Unified gas-kinetic wave-particle method for three-dimensional simulation of gas-particle fluidized bed

Xiaojian Yang [a], Yufeng Wei [b], Wei Shyy [a], Kun Xu [a,b,c,d,*]

[a] Department of Mechanical and Aerospace Engineering, Hong Kong University of Science and Technology, Clear Water Bay, Kowloon, Hong Kong, China
[b] Department of Mathematics, Hong Kong University of Science and Technology, Clear Water Bay, Kowloon, Hong Kong, China
[c] Shenzhen Research Institute, Hong Kong University of Science and Technology, Shenzhen, China
[d] Guangdong-Hong Kong-Macao Joint Laboratory for Data-Driven Fluid Mechanics and Engineering Applications, Hong Kong University of Science and Technology, Hong Kong, China

ARTICLE INFO

Keywords:
Gas–solid particle two phase flow
UGKWP
Gas-kinetic scheme
Gas–solid fluidization

ABSTRACT

The gas–solid particle two-phase flow in a fluidized bed shows complex physics. The multi-scale algorithm composed of the coupled gas-kinetic scheme (GKS) for the gas phase and unified gas-kinetic wave-particle method (UGKWP) for the solid particle phase is developed for three-dimensional fluidized bed study. For the solid-particle phase, different from the widely-used Eulerian and Lagrangian approaches, the UGKWP unifies the wave (dense particle region) and discrete particle (dilute particle region) formulation seamlessly according to a continuous variation of particle cell's Knudsen number (Kn). The GKS-UGKWP for the coupled gas-particle evolution system can automatically become an Eulerian–Eulerian (EE) method in the high particle collision regime and Eulerian–Lagrangian (EL) formulation in the collisionless particle regime. In the transition regime, the UGKWP can achieve a smooth transition between the Eulerian and Lagrangian limiting formulation. More importantly, the weights of mass distributions from analytical wave and discrete particle are related to the local Kn by $(1-\exp(-1/\mathrm{Kn}))$ for wave and $\exp(-1/\mathrm{Kn})$ for discrete particle. The UGKWP provides an optimal modeling in capturing the particle phase in difference regimes with the full consideration of physical accuracy and numerical efficiency. In the numerical simulation, the UGKWP does not need any prior division of dilute/dense regions, which makes it suitable for the fluidized bed problem, where the dilute/transition/dense regions instantaneously coexist and are dynamically interconvertible. In this paper, based on the GKS-UGKWP formulation two lab-scale fluidization cases, i.e., one turbulent fluidized bed and one circulating fluidized bed, are simulated in 3D and the simulation results are compared with the experimental measurements. The typical heterogeneous flow features of the fluidized bed are well captured and the statistics are in good agreement with experiment data.

1. Introduction

Gas–solid particle fluidization system is widely used in the energy and chemical industry. The vigorous interaction between gas and solid particle involves complex dynamics in the determination of mass and heat transfer [1]. Generally, the fluidization occurs in a container with a large number of solid particles and gas flow blown from below. This two-phase system usually shows rich and complex physics, such as the particle transport and collision, the clustering and dispersion of large number of particles, and the coexistence of dilute, transition, and dense regions, etc. For such a complex system, the prediction through an analytical solution is almost impossible, and the experiment measurement is expensive and depends highly on the measuring devices. Therefore, computational fluid dynamics (CFD) becomes a powerful and indispensable way for studying and understanding dynamics in fluidization, and guides the design and optimization of fluidized beds, etc [1–3].

Many numerical methods have been constructed to simulate gas–solid particle fluidization. The Eulerian–Eulerian (EE) approach, also called two fluid model (TFM), is one of the important approaches used in fluidization engineering [4,5]. In the EE approach, both gas and solid particle phases are described under the Eulerian framework. The kinetic theory for granular flow (KTGF) is one representative method of TFM, in which the constitutive relationship, i.e., the stress tensor, can be derived based on the Chapman–Enskog asymptotic analysis [5–7]. In general, the underlying assumption in TFM is that the solid phase stays in a near equilibrium state. In other words, with the slight

* Corresponding author at: Department of Mathematics, Hong Kong University of Science and Technology, Clear Water Bay, Kowloon, Hong Kong, China.
E-mail addresses: xyangbm@connect.ust.hk (X. Yang), yweibe@connect.ust.hk (Y. Wei), weishyy@ust.hk (W. Shyy), makxu@ust.hk (K. Xu).

https://doi.org/10.1016/j.cej.2022.139541
Received 29 June 2022; Received in revised form 14 September 2022; Accepted 29 September 2022
Available online 10 October 2022
1385-8947/

deviation from local Maxwellian distribution for the particle phase, the corresponding hydrodynamic evolution equations based on the macroscopic variables (density, velocity, and granular temperature) can be obtained. In reality, the solid particle phase can be in equilibrium or non-equilibrium state according to the Knudsen number (Kn), which is defined by the ratio of the particle mean free path over the characteristic length scale [8,9]. The solid phase stays in an equilibrium state at small Kn number under the intensive inter-particle collisions. This is likely to occur in the dense particle region in the gas-particle fluidization system. At large Kn number, the particle keeps the non-equilibrium state and the particle free transport plays a key role in the evolution, such as the dilute particle region. One of the outstanding non-equilibrium phenomenon is the particle trajectory crossing (PTC), where multiple particle velocities have to be captured at the same space location. The averaged single fluid velocity model in TFM has difficulty to give an accurate prediction of non-equilibrium physics [8]. Another alternative approach is Eulerian–Lagrangian (EL) method, such as the computational fluid dynamic-discrete element method (CFD-DEM), where all solid particles are tracked explicitly in the evolution [10,11]. To improve the computational efficiency with limited number of tractable particles, the numerical parcel concept for grouping many particles with the same property is employed in the coarse graining particle method (CGPM) [12,13], and multiphase particle-in-cell (MP-PIC) [14], etc. EL approach is theoretically able to give an accurate prediction of solid phase evolution in all regimes, but the computation cost increases gigantically in the dense particular flow region to track the tremendous amount of solid particles or parcels and follow their inter-particle collisions [2,15]. At current stage, the implementation of EL approach for industrial fluidization system is almost infeasible computationally, and the TFM is still the mainstream method in engineering applications [16]. In addition, the hybrid method that couples EE and EL approaches in different regions is studied in hope of maintaining both accuracy and efficiency in the simulation. The coupling strategy between EE/EL approaches plays an important role in order to achieve a smooth transition and give a reliable prediction [17,18]. Besides, other methods used for gas–solid fluidization system have been explored in the community, such as direct numerical simulation (DNS) [19–21], method of moment (MOM) [8,22], and material point method (MPM) [23], etc.

To capture the non-equilibrium physics of particular flow, a multiscale numerical method GKS-UGKWP for gas-particle two-phase system has been proposed, where the gas-kinetic scheme (GKS) is used for gas phase and unified gas-kinetic wave-particle method (UGKWP) for solid particle phase with dynamic coupling between them [24,25]. UGKWP is a wave-particle version of the unified gas-kinetic scheme (UGKS) for multiscale flow dynamics simulations [26,27]. UGKS is a direct modeling method on the scale of cell size and time step and captures the flow physics according to the cell's Kn number. It has been used for flow simulation in all regimes from the free molecular flow to the continuum Navier–Stokes solution. Based on the same methodology, UGKS is also successfully extended to other multiscale transport problems, such as radiative heat transfer, plasma, particular flow, etc [28–30]. In UGKS, both macroscopic flow variables and microscopic distribution function with discrete particle velocity points are updated in a deterministic way. Later, in order to improve the efficiency of UGKS, especially for the hypersonic flow computation, a particle-based UGKS, i.e., the so-called unified gas-kinetic particle (UGKP) method, has been proposed by updating the distribution function through stochastic particle [31,32]. In UGKP, the particles are categorized as free transport particles and collisional particles. The collisionless particle will be tracked in the whole time step; while the collisional one is only tracked before the first collision and eliminated within the time step. At the beginning of next time step, all annihilated particles will be re-sampled from an equilibrium state determined by the updated macroscopic flow variables within each control volume (cell). Furthermore, depending on the cell's Kn number, in the next time step a proportion of $(1\text{-}e^{-1/\mathrm{Kn}})$ re-sampled particles in UGKP from the equilibrium state will get collision and be eliminated again. More importantly, it is realized that the contribution from these re-sampled particles to the flux function in a finite volume scheme can be evaluated analytically through a wave or field-type representation. Therefore, in UGKP only the free transport particles need to be sampled and tracked in the next whole time step. The scheme with analytical formulation for the flux transport from those collisional particles is called unified gas-kinetic wave-particle (UGKWP) method. Tremendous reduction in computation cost and memory requirement is achieved in UGKWP for high speed flow computations, especially in the transition and near continuum flow regimes [31–34]. UGKWP is intrinsically suitable for capturing the multiscale non-equilibrium solid particle transport in the gas-particle two phase flow. At a very small cell Kn, no particles will be sampled in UGKWP, and the hydrodynamic formulation for solid particle evolution will automatically emerge. As a result, GKS-UGKWP method will go to the EE approach. On the contrary, at a large cell Kn, such as the collisionless regime, the evolution of the solid phase is fully tracked in the particle transport, and the GKS-UGKWP becomes the EL method. At an intermediate Kn, both wave and particle formulations in UGKWP contribute the solid phase's evolution, and the number of the sampled particles in UGKWP depends on the local cell's Kn, which ensures a smooth transition between different regimes. In addition, in the continuum regime, the particle phase from UGKWP will automatically converge to the kinetic theory-based Navier–Stokes flow solver, the so-called gas-kinetic scheme (GKS), which is validated in the flow, acoustic wave, and turbulence simulation, etc [35–39]. In the gas–solid particle fluidization, the GKS is also employed for the gas phase with assumption of continuum flow. Therefore, the limiting EE model from GKS-UGKWP will become GKS-GKS for the coupled two fluid phases. In conclusion, due to the coexistence of dilute/transition/dense solid particle regimes, the multiscale GKS-UGKWP can recover EE and EL formulations seamlessly in a single gas-particle two phase flow simulation.

In the gas–solid particle two phase flow, the accurate evaluation of inter-phase interaction is also essential for the accurate simulation of fluidization. The momentum and energy exchange between gas and solid phases due to the phase interaction is modeled through the drag force, buoyancy force, etc [7,8]. Among them, drag force plays the dominant role [40,41]. The hybrid model proposed by Gidaspow can be used for both dilute and dense solid particle regimes, and is widely accepted and employed in fluidization simulation [7]. Due to the heterogeneous property of gas–solid fluidization, such as the existence of clustering, the drag model modified by a scaling factor was proposed for the further improvement of accuracy [40,42,43]. In addition, the energy-minimization multiscale (EMMS) theory was successfully developed to model the heterogeneous structures in the gas–solid fluidization problem [44]. As an extension of the original EMMS method, the EMMS drag model, including the effect of local heterogeneous flow structures through EMMS theory, was proposed and successfully employed in the gas–solid fluidization simulation from the schemes, such as TFM, MP-PIC, etc [16,45–49]. Generally, for all these approaches it is essential to employ an accurate drag model in order to get reliable prediction for the gas-particle flow under the fluidized bed condition.

In this paper, two lab-scale fluidized bed problems, i.e., the turbulent fluidized bed from Gao et al. [40] and the circulating fluidized bed from Horio et al. [50], are calculated in three-dimensional space by GKS-UGKWP, and the numerical results are compared with the experimental measurements. The paper is organized as follows. Section 2 introduces the governing equations for the particle phase and UGKWP method. Then, Section 3 introduces the governing equations for the gas phase and GKS method. Section 4 introduces the numerical experiments, where the above two problems will be studied by GKS-UGKWP. The last section is the conclusion.

2. UGKWP for solid-particle phase

2.1. Governing equation for particle phase

The evolution of particle phase is governed by the following kinetic equation,

$$\frac{\partial f_s}{\partial t} + \nabla_x \cdot (\mathbf{u} f_s) + \nabla_u \cdot (\mathbf{a} f_s) = \frac{g_s - f_s}{\tau_s}, \tag{1}$$

where f_s is the distribution function of particle phase, $\mathbf{u}$ is the particle velocity, $\mathbf{a}$ is the particle acceleration caused by the external force, ∇_x is the divergence operator with respect to space, ∇_u is the divergence operator with respect to velocity, τ_s is the relaxation time for the particle phase. The equilibrium state g_s is,

$$g_s = \epsilon_s \rho_s \left(\frac{\lambda_s}{\pi}\right)^{\frac{3}{2}} e^{-\lambda_s[(\mathbf{u}-\mathbf{U}_s)^2]},$$

where ϵ_s is the volume fraction of particle phase, ρ_s is the material density of particle phase, λ_s is the value relevant to the granular temperature θ with $\lambda_s = \frac{1}{2\theta}$, and $\mathbf{U}_s$ is the macroscopic velocity of particle phase. The sum of kinetic and thermal energy for colliding particle may not be conserved due to the inelastic collision between particles. Therefore the collision term in Eq. (1) should satisfy the following compatibility condition [30],

$$\frac{1}{\tau_s}\int g_s \boldsymbol{\psi} \mathrm{d}\mathbf{u} = \frac{1}{\tau_s}\int f_s \boldsymbol{\psi}' \mathrm{d}\mathbf{u}, \tag{2}$$

where $\boldsymbol{\psi} = \left(1, \mathbf{u}, \frac{1}{2}\mathbf{u}^2\right)^T$ and $\boldsymbol{\psi}' = \left(1, \mathbf{u}, \frac{1}{2}\mathbf{u}^2 + \frac{e^2-1}{2}(\mathbf{u}-\mathbf{U}_s)^2\right)^T$. By Eq. (2), the lost energy due to the inelastic collision in 3D can be determined,

$$Q_{loss} = \frac{(1-e^2)\,3p_s}{2}, \tag{3}$$

where $e \in [0,1]$ is the restitution coefficient for determining the percentage of lost energy in inelastic collision. While $e = 1$ means no energy loss (elastic collision), $e = 0$ refers to total loss of all internal energy of particle phase $\epsilon_s \rho_s e_s = \frac{3}{2} p_s$ with $p_s = \frac{\epsilon_s \rho_s}{2\lambda_s}$. The accuracy of the above model for lost energy due to inelastic collisions depends on the e, which depends on the material properties of solid particles. Besides, it is worth noting that the solid particles studied in the current model are assumed to be spherical.

The particle acceleration $\mathbf{a}$ is determined by the external force, including the force reflecting the inter-phase interaction. In this paper, the drag force $\mathbf{D}$, the buoyancy force $\mathbf{F}_b$, and gravity $\mathbf{G}$ are considered. Here $\mathbf{D}$ and $\mathbf{F}_b$ are inter-phase force, standing for the force applied on the solid particles by gas flow. The general form of drag force can be written as,

$$\mathbf{D} = \frac{m_s}{\tau_{st}}\left(\mathbf{U}_g - \mathbf{u}\right), \tag{4}$$

where $m_s = \rho_s \frac{4}{3}\pi\left(\frac{d_s}{2}\right)^3$ is the mass of one particle, d_s is the diameter of solid particle, $\mathbf{U}_g$ is the macroscopic velocity of gas phase, and τ_{st} is the particle internal response time. The more commonly-used parameter in the drag model is β, called the inter-phase momentum transfer coefficient, with the relation to τ_{st} by $\beta = \frac{\epsilon_s \rho_s}{\tau_{st}}$. The accurate evaluation of drag plays key roles for the prediction of gas–solid fluidization. Many studies about the modeling of drag force have been conducted, such as the widely-accepted model by Gidaspow [7], the modified drag model through a scaling factor [40,42,43], the EMMS-based drag model [46–48], etc. Different drag models can be employed in GKS-UGKWP, and the drag model particularly used in this paper will be introduced in detail later.

Another interactive force considered is the buoyancy force, which can be modeled as,

$$\mathbf{F}_b = -\frac{m_s}{\rho_s}\nabla_x p_g, \tag{5}$$

where p_g is the pressure of gas phase. Then, the particle's acceleration can be obtained as,

$$\mathbf{a} = \frac{\mathbf{D} + \mathbf{F}_b}{m_s} + \mathbf{G}.$$

2.2. UGKWP method

In this subsection, the UGKWP for the evolution of solid particle phase is introduced. Generally, the kinetic equation of particle phase Eq. (1) is split as,

$$\mathcal{L}_{s1}: \quad \frac{\partial f_s}{\partial t} + \nabla_x \cdot (\mathbf{u} f_s) = \frac{g_s - f_s}{\tau_s}, \tag{6}$$

$$\mathcal{L}_{s2}: \quad \frac{\partial f_s}{\partial t} + \nabla_u \cdot (\mathbf{a} f_s) = 0, \tag{7}$$

and splitting operator is used to solve Eq. (1). Firstly, we focus on $\mathcal{L}_{s1}$ part, the particle phase kinetic equation without external force,

$$\frac{\partial f_s}{\partial t} + \nabla_x \cdot (\mathbf{u} f_s) = \frac{g_s - f_s}{\tau_s}.$$

For brevity, the subscript s standing for the solid particle phase will be neglected in this subsection. The integration solution of the kinetic equation can be written as,

$$f(\mathbf{x}, t, \mathbf{u}) = \frac{1}{\tau}\int_0^t g(\mathbf{x}', t', \mathbf{u}) e^{-(t-t')/\tau} \mathrm{d}t' \qquad + e^{-t/\tau} f_0(\mathbf{x} - \mathbf{u}t, \mathbf{u}), \tag{8}$$

where $\mathbf{x}' = \mathbf{x} + \mathbf{u}(t' - t)$ is the trajectory of particles, f_0 is the initial gas distribution function at time $t = 0$, and g is the corresponding equilibrium state.

In UGKWP, both macroscopic conservative variables and microscopic gas distribution function will be updated. Generally, in the finite volume framework, the cell-averaged macroscopic variables $\mathbf{W}_i$ of cell i can be updated by the conservation law,

$$\mathbf{W}_i^{n+1} = \mathbf{W}_i^n - \frac{1}{\Omega_i}\sum_{S_{ij}\in\partial\Omega_i} \mathbf{F}_{ij} S_{ij} + \Delta t \mathbf{S}_i, \tag{9}$$

where $\mathbf{W}_i = \left(\rho_i, \rho_i \mathbf{U}_i, \rho_i E_i\right)$ is the cell-averaged macroscopic variables,

$$\mathbf{W}_i = \frac{1}{\Omega_i}\int_{\Omega_i} \mathbf{W}(\mathbf{x})\,\mathrm{d}\Omega,$$

Ω_i is the volume of cell i, $\partial\Omega_i$ denotes the set of cell interfaces of cell i, S_{ij} is the area of the jth interface of cell i, $\mathbf{F}_{ij}$ denotes the macroscopic fluxes across the interface S_{ij}, which can be written as

$$\mathbf{F}_{ij} = \int_0^{\Delta t}\int \mathbf{u}\cdot\mathbf{n}_{ij} f_{ij}(\mathbf{x}, t, \mathbf{u})\boldsymbol{\psi}\mathrm{d}\mathbf{u}\mathrm{d}t, \tag{10}$$

where $\mathbf{n}_{ij}$ is the normal unit vector of interface S_{ij}, $f_{ij}(t)$ is the time-dependent distribution function on the interface S_{ij}, and $\boldsymbol{\psi} = (1, \mathbf{u}, \frac{1}{2}\mathbf{u}^2)^T$. $\mathbf{S}_i$ is the source term due to inelastic collision inside each control volume, where the solid-particle's internal energy has not been taken into account in the above equation.

Substituting the time-dependent distribution function Eq. (8) into Eq. (10), the fluxes can be obtained,

$$\begin{aligned}
\mathbf{F}_{ij} &= \int_0^{\Delta t}\int \mathbf{u}\cdot\mathbf{n}_{ij} f_{ij}(\mathbf{x}, t, \mathbf{u})\boldsymbol{\psi}\mathrm{d}\mathbf{u}\mathrm{d}t \\
&= \int_0^{\Delta t}\int \mathbf{u}\cdot\mathbf{n}_{ij}\left[\frac{1}{\tau}\int_0^t g(\mathbf{x}', t', \mathbf{u}) e^{-(t-t')/\tau}\mathrm{d}t'\right]\boldsymbol{\psi}\mathrm{d}\mathbf{u}\mathrm{d}t \\
&+ \int_0^{\Delta t}\int \mathbf{u}\cdot\mathbf{n}_{ij}\left[e^{-t/\tau} f_0(\mathbf{x} - \mathbf{u}t, \mathbf{u})\right]\boldsymbol{\psi}\mathrm{d}\mathbf{u}\mathrm{d}t \\
&\overset{def}{=} \mathbf{F}_{ij}^{eq} + \mathbf{F}_{ij}^{fr}.
\end{aligned}$$

The procedure of obtaining the local equilibrium state g_0 at the cell interface as well as the construction of $g(t)$ is the same as that in GKS [35]. For a second-order accuracy, the equilibrium state g around the cell interface is written as,

$$g\left(\mathbf{x}', t', \mathbf{u}\right) = g_0\left(\mathbf{x}, \mathbf{u}\right)\left(1 + \bar{\mathbf{a}}\cdot\mathbf{u}\left(t' - t\right) + \bar{A}t'\right),$$

where $\overline{\mathbf{a}} = \left[\overline{a_1}, \overline{a_2}, \overline{a_3}\right]^T$, $\overline{a_i} = \frac{\partial g}{\partial x_i}/g$, $i = 1, 2, 3$, $\overline{A} = \frac{\partial g}{\partial t}/g$, and g_0 is the local equilibrium on the interface. Specifically, the coefficients of spatial derivatives $\overline{a_i}$ can be obtained from the corresponding derivatives of the macroscopic variables,

$$\left\langle \overline{a_i} \right\rangle = \partial \mathbf{W}_0 / \partial x_i,$$

where $i = 1, 2, 3$, and $\langle ... \rangle$ means the moments of the Maxwellian distribution functions,

$$\langle ... \rangle = \int \boldsymbol{\psi} \left(... \right) g \mathrm{d}\mathbf{u}.$$

The coefficients of temporal derivative $\overline{A}$ can be determined by the compatibility condition,

$$\left\langle \overline{\mathbf{a}} \cdot \mathbf{u} + \overline{A} \right\rangle = \begin{bmatrix} 0 \\ \mathbf{0} \\ -\frac{Q_{loss}}{\tau_s} \end{bmatrix},$$

where $Q_{loss} = \frac{(1-e^2)3p_s}{2}$ is the energy lose due to particle–particle inelastic collision. Now, all the coefficients in the equilibrium state $g\left(\mathbf{x}', t', \mathbf{u}\right)$ have been determined, and its integration becomes,

$$\begin{aligned} f^{eq}(\mathbf{x}, t, \mathbf{u}) &\overset{def}{=} \frac{1}{\tau} \int_0^t g(\mathbf{x}', t', \mathbf{u}) e^{-(t-t')/\tau} \mathrm{d}t' \\ &= c_1 g_0 \left(\mathbf{x}, \mathbf{u}\right) + c_2 \overline{\mathbf{a}} \cdot \mathbf{u} g_0 \left(\mathbf{x}, \mathbf{u}\right) + c_3 A g_0 \left(\mathbf{x}, \mathbf{u}\right), \end{aligned} \tag{11}$$

with coefficients,

$$\begin{aligned} c_1 &= 1 - e^{-t/\tau}, \\ c_2 &= (t + \tau) e^{-t/\tau} - \tau, \\ c_3 &= t - \tau + \tau e^{-t/\tau}, \end{aligned}$$

and thereby the integrated flux over a time step for equilibrium state can be obtained,

$$\mathbf{F}_{ij}^{eq} = \int_0^{\Delta t} \int \mathbf{u} \cdot \mathbf{n}_{ij} f_{ij}^{eq}(\mathbf{x}, t, \mathbf{u}) \boldsymbol{\psi} \mathrm{d}\mathbf{u} \mathrm{d}t. \tag{12}$$

Besides, the flux contribution from the particle free transport f_0 in Eq. (8) is calculated by tracking the particles sampled from f_0. Therefore, the updating of the cell-averaged macroscopic variables can be written as,

$$\mathbf{W}_i^{n+1} = \mathbf{W}_i^n - \frac{1}{\Omega_i} \sum_{S_{ij} \in \partial \Omega_i} \mathbf{F}_{ij}^{eq} S_{ij} + \frac{\mathbf{w}_i^{fr}}{\Omega_i} + \Delta t \mathbf{S}_i, \tag{13}$$

where $\mathbf{w}_i^{fr}$ is the net free streaming flow of cell i, standing for the flux contribution of the free streaming of particles, and the term $\mathbf{S}_i = \left[0, \mathbf{0}, -\frac{Q_{loss}}{\tau_s}\right]^T$ is the source term due to the inelastic collision for solid particle phase.

The net free streaming flow $\mathbf{w}_i^{fr}$ is determined in the following. The evolution of particle should also satisfy the integral solution of the kinetic equation, which can be written as,

$$f(\mathbf{x}, t, \mathbf{u}) = \left(1 - e^{-t/\tau}\right) g^+(\mathbf{x}, t, \mathbf{u}) + e^{-t/\tau} f_0(\mathbf{x} - \mathbf{u}t, \mathbf{u}), \tag{14}$$

where g^+ is named as the hydrodynamic distribution function with analytical formulation. The initial distribution function f_0 has a probability of $e^{-t/\tau}$ to free transport and $(1 - e^{-t/\tau})$ to colliding with other particles. The post-collision particles satisfies the distribution $g^+(\mathbf{x}, \mathbf{u}, t)$. The free transport time before the first collision with other particles is denoted as t_c. The cumulative distribution function of t_c is,

$$F\left(t_c < t\right) = 1 - e^{-t/\tau}, \tag{15}$$

and therefore t_c can be sampled as $t_c = -\tau \ln(\eta)$, where η is a random number generated from a uniform distribution $U(0, 1)$. Then, the free streaming time t_f for each particle is determined separately by,

$$t_f = \min\left[-\tau \ln(\eta), \Delta t\right], \tag{16}$$

where Δt is the time step. Therefore, within one time step, all particles can be divided into two groups: the collisionless particle and the collisional particle, and they are determined by the relation between of time step Δt and free streaming time t_f. Specifically, if $t_f = \Delta t$ for one particle, it is collisionless one, and the trajectory of this particle is fully tracked in the whole time step. On the contrary, if $t_f < \Delta t$ for one particle, it is collisional particle, and its trajectory will be tracked until t_f. The collisional particle is eliminated at t_f in the simulation and the associated mass, momentum and energy carried by this particle are merged into the updated macroscopic quantities of all annihilated particles in the relevant cell. More specifically, the particle trajectory in the free streaming process within time t_f is tacked by,

$$\mathbf{x} = \mathbf{x}^n + \mathbf{u}^n t_f. \tag{17}$$

The term $\mathbf{w}_i^{fr}$ can be calculated by counting the particles passing through the interfaces of cell i,

$$\mathbf{w}_i^{fr} = \sum_{k \in P(\partial \Omega_i^+)} \boldsymbol{\phi}_k - \sum_{k \in P(\partial \Omega_i^-)} \boldsymbol{\phi}_k, \tag{18}$$

where $P\left(\partial \Omega_i^+\right)$ is the particle set moving into the cell i during one time step, $P\left(\partial \Omega_i^-\right)$ is the particle set moving out of the cell i during one time step, k is the particle index in one specific set, and $\boldsymbol{\phi}_k = \left[m_k, m_k \mathbf{u}_k, \frac{1}{2} m_k (\mathbf{u}_k^2)\right]^T$ is the mass, momentum and energy carried by particle k. Therefore, $\mathbf{w}_i^{fr}/\Omega_i$ is the net conservative quantities caused by the free stream of the tracked particles. Now, all the terms in Eq. (13) have been determined and the macroscopic variables $\mathbf{W}_i$ can be updated.

The trajectories of all particles have been tracked during the time interval $\left(0, t_f\right)$. For the collisionless particles with $t_f = \Delta t$, they still survive at the end of one time step; while the collisional particles with $t_f < \Delta t$ are deleted after their first collision and they are supposed to go to the equilibrium state in that cell. Therefore, the macroscopic variables of the collisional particles in cell i at the end of each time step can be directly obtained based on the conservation law,

$$\mathbf{W}_i^h = \mathbf{W}_i^{n+1} - \mathbf{W}_i^p, \tag{19}$$

where $\mathbf{W}_i^{n+1}$ is the updated conservative variables in Eq. (13) and $\mathbf{W}_i^p$ are the mass, momentum, and energy of remaining collisionless particles in the cell at the end of the time step. Besides, the macroscopic variables $\mathbf{W}_i^h$ account for all eliminated collisional particles to the equilibrium state, and these particles can be re-sampling from $\mathbf{W}_i^h$ based on the overall Maxwellian distribution at the beginning of the next time step. Now the updates of both macroscopic variables and the microscopic particles have been presented. The above method is the so-called unified gas-kinetic particle (UGKP) method.

The above UGKP can be further developed to UGKWP method. In UGKP method, all particles are divided into collisionless and collisional particles in each time step. The collisional particles are deleted after the first collision and re-sampled from $\mathbf{W}_i^h$ at the beginning of the next time step. However, only the collisionless part of the re-sampled particles can survive in the next time step, and all collisional ones will be deleted again. Actually, the transport fluxes from these collisional particles can be evaluated analytically without using particles. According to the cumulative distribution Eq. (15), the proportion of the collisionless particles is $e^{-\Delta t/\tau}$, and therefore in UGKWP only the collisionless particles from the hydrodynamic variables $\mathbf{W}_i^h$ in cell i will be re-sampled with the total mass, momentum, and energy,

$$\mathbf{W}_i^{hp} = e^{-\Delta t/\tau} \mathbf{W}_i^h. \tag{20}$$

Then, the free transport time of all the re-sampled particles will be $t_f = \Delta t$ in UGKWP. The fluxes $\mathbf{F}^{fr,wave}$ from these un-sampled collisional particle of $(1 - e^{-\Delta t/\tau})\mathbf{W}_i^h$ can be evaluated analytically [31,32]. Now, same as UGKP, the net flux $\mathbf{w}_i^{fr,p}$ accounting for the free streaming of the particles across cell interfaces includes the contribution from

the remaining particles from previous time step and the re-sampled collisionless ones from $\mathbf{W}_i^{hp}$,

$$\mathbf{w}_i^{fr,p} = \sum_{k\in P(\partial\Omega_i^+)} \boldsymbol{\phi}_k - \sum_{k\in P(\partial\Omega_i^-)} \boldsymbol{\phi}_k. \tag{21}$$

Then, the macroscopic flow variables in UGKWP are updated by

$$\mathbf{W}_i^{n+1} = \mathbf{W}_i^n - \frac{1}{\Omega_i}\sum_{S_{ij}\in\partial\Omega_i} \mathbf{F}_{ij}^{eq} S_{ij} - \frac{1}{\Omega_i}\sum_{S_{ij}\in\partial\Omega_i} \mathbf{F}_{ij}^{fr,wave} S_{ij} + \frac{\mathbf{w}_i^{fr,p}}{\Omega_i} + \Delta t\mathbf{S}_i, \tag{22}$$

where $\mathbf{F}_{ij}^{fr,wave}$ is the flux function from the un-sampled collisional particles [28,31,32], which can be written as,

$$\begin{aligned}\mathbf{F}_{ij}^{fr,wave} &= \mathbf{F}_{ij}^{fr,UGKS}(\mathbf{W}_i^h) - \mathbf{F}_{ij}^{fr,DVM}(\mathbf{W}_i^{hp}) \\ &= \int_0^{\Delta t}\int \mathbf{u}\cdot\mathbf{n}_{ij}\left[e^{-t/\tau} f_0(\mathbf{x}-\mathbf{u}t,\mathbf{u})\right]\boldsymbol{\psi}\mathrm{d}\mathbf{u}\mathrm{d}t \\ &- e^{-\Delta t/\tau}\int_0^{\Delta t}\int \mathbf{u}\cdot\mathbf{n}_{ij}\left[g_0^h(\mathbf{x},\mathbf{u}) - t\mathbf{u}\cdot g_{\mathbf{x}}^h(\mathbf{x},\mathbf{u})\right]\boldsymbol{\psi}\mathrm{d}\mathbf{u}\mathrm{d}t \\ &= \int \mathbf{u}\cdot\mathbf{n}_{ij}\left[\left(q_4 - \Delta t e^{-\Delta t/\tau}\right) g_0^h(\mathbf{x},\mathbf{u}) + \left(q_5 + \frac{\Delta t^2}{2}e^{-\Delta t/\tau}\right)\mathbf{u}\right. \\ &\left.\cdot g_{\mathbf{x}}^h(\mathbf{x},\mathbf{u})\right]\boldsymbol{\psi}\mathrm{d}\mathbf{u},\end{aligned} \tag{23}$$

with the coefficients,

$$q_4 = \tau\left(1-e^{-\Delta t/\tau}\right),$$
$$q_5 = \tau\Delta t e^{-\Delta t/\tau} - \tau^2\left(1-e^{-\Delta t/\tau}\right).$$

The source term $\mathbf{S}_i$ in Eq. (22) is solved in an implicit way, which means

$$\rho_i^{n+1}E_i^{n+1} = \rho_i^n E_i^n + S_i^{n+1},$$

where

$$\rho_i^n E_i^n = \frac{1}{2}\rho_i^n\left(\mathbf{U}_i^n\right)^2 + \frac{3}{2}p_{s,i}^n,$$
$$\rho_i^{n+1}E_i^{n+1} = \frac{1}{2}\rho_i^{n+1}\left(\mathbf{U}_i^{n+1}\right)^2 + \frac{3}{2}p_{s,i}^{n+1},$$

and

$$S_i^{n+1} = -\frac{3\left(1-e^2\right)}{2}\frac{\Delta t}{\tau_s}p_{s,i}^{n+1}, \tag{24}$$

by which the $p_{s,i}^{n+1}$ can by obtained,

$$p_{s,i}^{n+1} = \frac{\frac{3}{2}p_{s,i}^n + \frac{1}{2}\rho_i^n\left(\mathbf{U}_i^n\right)^2 - \frac{1}{2}\rho_i^{n+1}\left(\mathbf{U}_i^{n+1}\right)^2}{\frac{3}{2} + \frac{3(1-e^2)}{2}\frac{\Delta t}{\tau_s}}, \tag{25}$$

and further $\rho_i^{n+1}E_i^{n+1}$ is updated. Up to now, the first part $\mathcal{L}_{s1}$ has been updated.

The second part $\mathcal{L}_{s2}$ in Eq. (7) accounts for the external acceleration,

$$\frac{\partial f_s}{\partial t} + \nabla_u\cdot\left(\mathbf{a}f_s\right) = 0,$$

where the velocity-dependent acceleration term caused by inter-phase forces and solid particle's gravity has the following form,

$$\mathbf{a} = \frac{\mathbf{U}_g - \mathbf{u}}{\tau_{st}} - \frac{1}{\rho_s}\nabla_x p_g + \mathbf{G}.$$

Taking moment $\boldsymbol{\psi}$ to Eq. (7),

$$\int\boldsymbol{\psi}\left(\frac{\partial f_s}{\partial t} + \mathbf{a}\cdot\nabla_u f_s + f_s\nabla_u\cdot\mathbf{a}\right)\mathrm{d}\mathbf{u} = 0,$$

and in the Euler regime with $f_s = g_s + \mathcal{O}(\tau_s)$, we can obtain,

$$\frac{\partial\mathbf{W}_s}{\partial t} + \mathbf{Q}_s = 0,$$

where

$$\mathbf{W}_s = \begin{bmatrix}\epsilon_s\rho_s \\ \epsilon_s\rho_s\mathbf{U}_s \\ \epsilon_s\rho_s E_s\end{bmatrix},$$

$$\mathbf{Q}_s = \begin{bmatrix}0 \\ \frac{\epsilon_s\rho_s(\mathbf{U}_s-\mathbf{U}_g)}{\tau_{st}} + \epsilon_s\nabla_x p_g - \epsilon_s\rho_s\mathbf{G} \\ \frac{\epsilon_s\rho_s\mathbf{U}_s\cdot(\mathbf{U}_s-\mathbf{U}_g)}{\tau_{st}} + 3\frac{p_s}{\tau_{st}} + \epsilon_s\mathbf{U}_s\cdot\nabla_x p_g - \epsilon_s\rho_s\mathbf{U}_s\cdot\mathbf{G}\end{bmatrix}.$$

When the first-order forward Euler method is employed for time marching, the cell-averaged macroscopic variable can be updated by,

$$\mathbf{W}_s^{n+1} = \mathbf{W}_s - \mathbf{Q}_s\Delta t, \tag{26}$$

Note that the $\mathbf{W}_s$ represents the macroscopic variables after updating the $\mathcal{L}_{s1}$ part. Besides, the modifications on velocity and location of the remaining free transport particles can be written as,

$$\mathbf{u}^{n+1} = \mathbf{u} + \mathbf{a}t_f, \tag{27}$$

$$\mathbf{x}^{n+1} = \mathbf{x} + \frac{\mathbf{a}}{2}t_f^2. \tag{28}$$

Now the update of the solid particle phase in one time step has been finished. In the following, specific variables determination for the solid-particle phase will be presented.

2.3. Particle phase Knudsen number

The particle phase Kn number is defined by the ratio of collision time τ_s to the characteristic time of macroscopic flow t_{ref},

$$\mathrm{Kn} = \frac{\tau_s}{t_{ref}}, \tag{29}$$

where t_{ref} is the characteristic time, defined as the ratio of flow characteristic length to the flow characteristic velocity, $t_{ref} = L_{ref}/U_{ref}$, and τ_s is the time interval between collisions of solid particles. In this paper, τ_s is taken as [8,51],

$$\tau_s = \frac{\sqrt{\pi}d_s}{12\epsilon_s g_r\sqrt{\theta}}, \tag{30}$$

where d_s is the diameter of solid particle, ϵ_s is the volume fraction of solid phase, θ is the granular temperature. g_r is the radial distribution function with the following form,

$$g_r = \frac{2-c}{2(1-c)^3}, \tag{31}$$

where $c = \epsilon_s/\epsilon_{s,max}$ is the ratio of the volume fraction ϵ_s to the allowed maximum value $\epsilon_{s,max}$. A typical feature of the gas–solid flow in fluidized bed is that the instantaneously coexistence of the dilute and dense zones. Generally, in the dilute zone, the collision frequency between solid particles is low, leading to a large Kn, and in UGKWP particles will be sampled and tracked to model the transport behavior of solid particles; on the contrary, for the dense flow, the high-frequency inter-particle collisions usually make the solid phase in equilibrium state, so in UGKWP the evolution can be fully determined the wave formula in Eq. (22), and there is no need for particle sampling. The solid particles' behaviors and flow states can be directly modeled in the UGKWP based on Kn, ensuring the consistence of numerical scheme with flow physics. More specifically, the particle free transport and collision dynamics in UGKWP is mainly determined by the ratio of τ_s to the numerical time step Δt, and the cell's Knudsen number is defined by $\mathrm{Kn} = \tau/\Delta t$.

2.4. Hydrodynamic equations in continuum flow regime

When the collision between solid particles are elastic with $e = 1$, in the continuum flow regime with $f_s = g_s + \mathcal{O}(\tau_s)$, the hydrodynamic equations becomes the Euler equations coupled with the

momentum and energy exchange terms, which can be obtained based on the Chapman–Enskog asymptotic analysis for the kinetic equation Eq. (1) [52],

$$\begin{aligned}
&\frac{\partial\left(\epsilon_s\rho_s\right)}{\partial t}+\nabla_x\cdot\left(\epsilon_s\rho_s\mathbf{U}_s\right)=0,\\
&\frac{\partial\left(\epsilon_s\rho_s\mathbf{U}_s\right)}{\partial t}+\nabla_x\cdot\left(\epsilon_s\rho_s\mathbf{U}_s\mathbf{U}_s+p_s\mathbb{I}\right)=\frac{\epsilon_s\rho_s\left(\mathbf{U}_g-\mathbf{U}_s\right)}{\tau_{st}}-\epsilon_s\nabla_x p_g+\epsilon_s\rho_s\mathbf{G},\\
&\frac{\partial\left(\epsilon_s\rho_s E_s\right)}{\partial t}+\nabla_x\cdot\left(\left(\epsilon_s\rho_s E_s+p_s\right)\mathbf{U}_s\right)\\
&=\frac{\epsilon_s\rho_s\mathbf{U}_s\cdot\left(\mathbf{U}_g-\mathbf{U}_s\right)}{\tau_{st}}-\frac{3p_s}{\tau_{st}}-\epsilon_s\mathbf{U}_s\cdot\nabla_x p_g+\epsilon_s\rho_s\mathbf{U}_s\cdot\mathbf{G}.
\end{aligned}\tag{32}$$

With the increasing of solid volume fraction, the inter-particle interaction becomes more complex, and a precise evaluation of solid phase's pressure becomes difficult. The pressure term p_s in Eq. (32) is the so-called kinetic pressure, which plays the dominant role in the dilute and moderately dense regime. Besides the kinetic pressure part p_s, the collisional pressure p_c closed by KTGF and the frictional pressure p_f reflecting the effect of enduring inter-particle contact and frictions are widely accepted and employed in TFM, which shows excellent performance in the gas–solid fluidization problems [4,6]. Many studies to improve the accuracy of pressure/stress terms are conducted [53–55]. To the authors' knowledge, however, no such a model has been proposed to give accurate kinetic/collisional/frictional pressure in a multi-scale solver for dilute/moderately dense/dense flow. So in this paper as the first attempt, the models of p_c and p_f widely used in TFM are directly added to the macroscopic variables in the UGKWP method. The collisional pressure p_c, proposed by Lun et al. [6], is widely employed in the gas–solid flow in fluidized beds, which is used in this paper and can be written as,

$$p_c=2\left(1+e\right)\epsilon_s^2\rho_s\theta g_r,\tag{33}$$

where e is the restitution coefficient, taken as 0.8 in this paper unless special notification, and g_r is the radial distribution function given by Eq. (31). The p_f accounts for the enduring inter-particle contacts and frictions, which plays important roles when the solid phase is in the near-packing state. Some models of p_f have been proposed [53,56,57]. In this paper, the correlation proposed by Johnson and Jackson is employed [56,58],

$$p_f=\begin{cases}0 & ,\epsilon_s\le\epsilon_{s,crit},\\ 0.1\epsilon_s\dfrac{\left(\epsilon_s-\epsilon_{s,crit}\right)^2}{\left(\epsilon_{s,max}-\epsilon_s\right)^5} & ,\epsilon_s>\epsilon_{s,crit},\end{cases}\tag{34}$$

where p_f is with unit of Pa. $\epsilon_{s,crit}$ is the critical volume fraction of particle flow, and it takes a value 0.5 in this paper unless special notification. In this paper, both p_c and p_f are considered to recover a more realistic physics. Finally, the momentum and energy equations under continuum limiting regime can be written as,

$$\begin{aligned}
&\frac{\partial\left(\epsilon_s\rho_s\mathbf{U}_s\right)}{\partial t}+\nabla_x\cdot\left(\epsilon_s\rho_s\mathbf{U}_s\mathbf{U}_s+p_s\mathbb{I}+p_c\mathbb{I}+p_f\mathbb{I}\right)\\
&=\frac{\epsilon_s\rho_s\left(\mathbf{U}_g-\mathbf{U}_s\right)}{\tau_{st}}-\epsilon_s\nabla_x p_g+\epsilon_s\rho_s\mathbf{G}.
\end{aligned}\tag{35}$$

$$\begin{aligned}
&\frac{\partial\left(\epsilon_s\rho_s E_s\right)}{\partial t}+\nabla_x\cdot\left(\left(\epsilon_s\rho_s E_s+p_s+p_c+p_f\right)\mathbf{U}_s\right)\\
&=\frac{\epsilon_s\rho_s\mathbf{U}_s\cdot\left(\mathbf{U}_g-\mathbf{U}_s\right)}{\tau_{st}}-\frac{3p_s}{\tau_{st}}-\epsilon_s\mathbf{U}_s\cdot\nabla_x p_g\\
&\qquad+\epsilon_s\rho_s\mathbf{U}_s\cdot\mathbf{G}.
\end{aligned}\tag{36}$$

The terms relevant to collisional pressure, $\nabla_x\cdot\left(p_c\mathbb{I}\right)$, $\nabla_x\cdot\left(p_c\mathbf{U}_s\right)$, and frictional pressure, $\nabla_x\cdot\left(p_f\mathbb{I}\right)$, $\nabla_x\cdot\left(p_f\mathbf{U}_s\right)$, are solved as source terms in this paper. To avoid the solid volume fraction ϵ_s exceeding its maximum value $\epsilon_{s,max}$, the flux limiting model near the packing condition, proposed in our previous work, is employed in UGKWP method for solid phase and is not reiterated here [25].

3. GKS for gas phase

3.1. Governing equation for gas phase

The gas phase is regarded as continuum flow and the governing equations are the Navier–Stokes equations with source terms reflecting the inter-phase interaction [7,59],

$$\begin{aligned}
&\frac{\partial\left(\widetilde{\rho_g}\right)}{\partial t}+\nabla_x\cdot\left(\widetilde{\rho_g}\mathbf{U}_g\right)=0,\\
&\frac{\partial\left(\widetilde{\rho_g}\mathbf{U}_g\right)}{\partial t}+\nabla_x\cdot\left(\widetilde{\rho_g}\mathbf{U}_g\mathbf{U}_g+\widetilde{p_g}\mathbb{I}\right)-\epsilon_g\nabla_x\cdot\left(\mu_g\boldsymbol{\sigma}\right)\\
&=p_g\nabla_x\epsilon_g-\frac{\epsilon_s\rho_s\left(\mathbf{U}_g-\mathbf{U}_s\right)}{\tau_{st}}+\rho_g\mathbf{G},\\
&\frac{\partial\left(\widetilde{\rho_g}E_g\right)}{\partial t}+\nabla_x\cdot\left(\left(\widetilde{\rho_g}E_g+\widetilde{p_g}\right)\mathbf{U}_g\right)-\epsilon_g\nabla_x\cdot\left(\mu_g\boldsymbol{\sigma}\cdot\mathbf{U}_g-\kappa\nabla_x T_g\right)=-p_g\frac{\partial\epsilon_g}{\partial t}\\
&\qquad-\frac{\epsilon_s\rho_s\mathbf{U}_s\cdot\left(\mathbf{U}_g-\mathbf{U}_s\right)}{\tau_{st}}+\frac{3p_s}{\tau_{st}}+\rho_g\mathbf{U}_g\cdot\mathbf{G},
\end{aligned}\tag{37}$$

where $\widetilde{\rho_g}=\epsilon_g\rho_g$ is the apparent density of gas phase, $p_g=\rho_g RT_g$ is the pressure of gas phase and $\widetilde{p_g}=\widetilde{\rho_g}RT_g$, the strain rate tensor $\boldsymbol{\sigma}$ is

$$\boldsymbol{\sigma}=\nabla_x\mathbf{U}_g+\left(\nabla_x\mathbf{U}_g\right)^T-\frac{2}{3}\nabla_x\cdot\mathbf{U}_g\mathbb{I},$$

and

$$\mu_g=\tau_g p_g,\qquad\kappa=\frac{5}{2}R\tau_g p_g.$$

In particular, at the right hand side in Eq. (37), the term $p_g\nabla_x\epsilon_g$ is called "nozzle" term, and the associated work term $-p_g\frac{\partial\epsilon_g}{\partial t}$ is called pDV work term, since it is similar to the pDV term in the quasi-one-dimensional gas nozzle flow equations [58]. Unphysical pressure fluctuations might occurs if the "nozzle" term and pDV term are not solved correctly. According to [60], Eq. (37) can be written as the following form,

$$\begin{aligned}
&\frac{\partial\left(\rho_g\right)}{\partial t}+\nabla_x\cdot\left(\rho_g\mathbf{U}_g\right)=C_{\epsilon_g}\rho_g,\\
&\frac{\partial\left(\rho_g\mathbf{U}_g\right)}{\partial t}+\nabla_x\cdot\left(\rho_g\mathbf{U}_g\mathbf{U}_g+p_g\mathbb{I}-\mu_g\boldsymbol{\sigma}\right)=C_{\epsilon_g}\rho_g\mathbf{U}_g-\frac{\epsilon_s\rho_s\left(\mathbf{U}_g-\mathbf{U}_s\right)}{\epsilon_g\tau_{st}}+\frac{\rho_g\mathbf{G}}{\epsilon_g},\\
&\frac{\partial\left(\rho_g E_g\right)}{\partial t}+\nabla_x\cdot\left(\left(\rho_g E_g+p_g\right)\mathbf{U}_g-\mu_g\boldsymbol{\sigma}\cdot\mathbf{U}_g+\kappa\nabla_x T_g\right)=C_{\epsilon_g}\left(\rho_g E_g+p_g\right)\\
&\qquad-\frac{\epsilon_s\rho_s\mathbf{U}_s\cdot\left(\mathbf{U}_g-\mathbf{U}_s\right)}{\epsilon_g\tau_{st}}+\frac{3p_s}{\epsilon_g\tau_{st}}+\frac{\rho_g\mathbf{U}_g\cdot\mathbf{G}}{\epsilon_g},
\end{aligned}\tag{38}$$

where, $C_{\epsilon_g}=-\frac{1}{\epsilon_g}\frac{\mathrm{d}\epsilon_g}{\mathrm{d}t}$ with $\frac{\mathrm{d}\epsilon_g}{\mathrm{d}t}=\frac{\partial\epsilon_g}{\partial t}+\mathbf{U}_g\cdot\nabla\epsilon_g$, and how to solve C_{ϵ_g} in this paper will be introduced later.

3.2. GKS for gas evolution

This subsection introduces the evolution of gas phase in gas-particle two-phase system. The gas flow is governed by the Navier–Stokes equations with the inter-phase interaction, and the corresponding GKS is a limiting scheme of UGKWP in the continuum flow regime. In general, the evolution of gas phase Eq. (38) can be split into two parts,

$$\mathcal{L}_{g1}:\begin{cases}\frac{\partial(\rho_g)}{\partial t}+\nabla_x\cdot\left(\rho_g\mathbf{U}_g\right)=0,\\ \frac{\partial(\rho_g\mathbf{U}_g)}{\partial t}+\nabla_x\cdot\left(\rho_g\mathbf{U}_g\mathbf{U}_g+p_g\mathbb{I}-\mu_g\boldsymbol{\sigma}\right)=0,\\ \frac{\partial(\rho_g E_g)}{\partial t}+\nabla_x\cdot\left(\left(\rho_g E_g+p_g\right)\mathbf{U}_g-\mu_g\boldsymbol{\sigma}\cdot\mathbf{U}_g+\kappa\nabla_x T_g\right)=0,\end{cases}\tag{39}$$

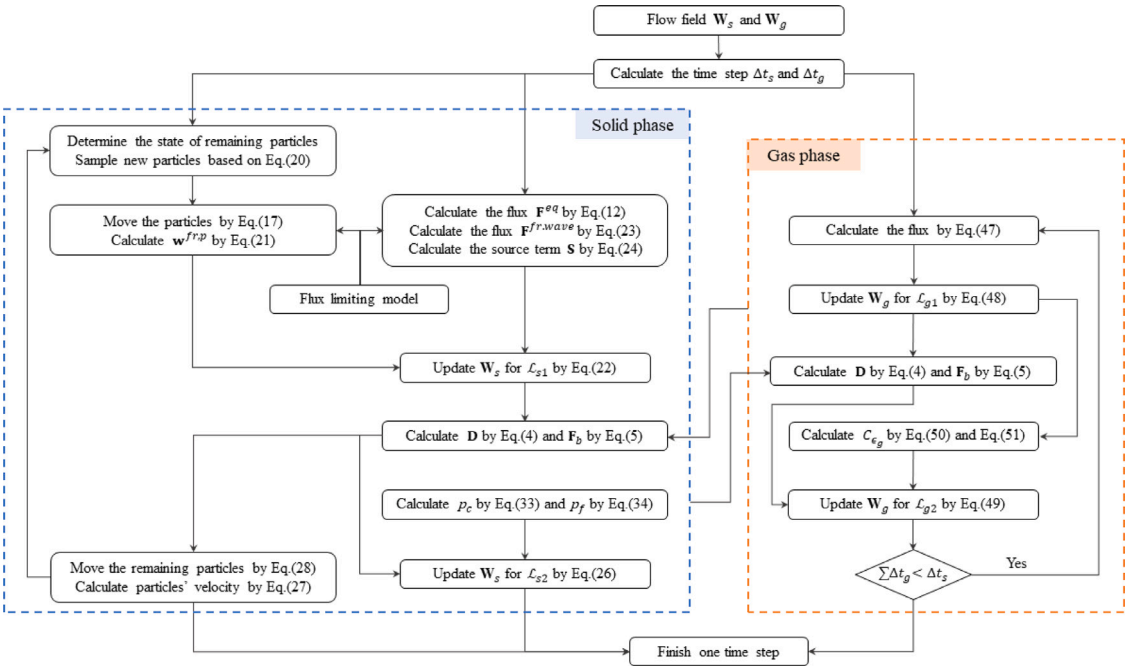

Fig. 1. The flow chart of GKS-UGKWP method.

$$\mathcal{L}_{g2}: \begin{cases} \frac{\partial(\rho_g)}{\partial t} = C_{\epsilon_g}\rho_g, \\ \frac{\partial(\rho_g \mathbf{U}_g)}{\partial t} = C_{\epsilon_g}\rho_g \mathbf{U}_g - \frac{\epsilon_s \rho_s (\mathbf{U}_g - \mathbf{U}_s)}{\epsilon_g \tau_{st}} + \frac{\rho_g \mathbf{G}}{\epsilon_g}, \\ \frac{\partial(\rho_g E_g)}{\partial t} = C_{\epsilon_g}\left(\rho_g E_g + p_g\right) - \frac{\epsilon_s \rho_s \mathbf{U}_s \cdot (\mathbf{U}_g - \mathbf{U}_s)}{\epsilon_g \tau_{st}} + \frac{3p_s}{\epsilon_g \tau_{st}} + \frac{\rho_g \mathbf{U}_g \cdot \mathbf{G}}{\epsilon_g}. \end{cases} \tag{40}$$

The GKS is constructed to solve $\mathcal{L}_{g1}$ and $\mathcal{L}_{g2}$ separately. Firstly, the kinetic equation without acceleration term for gas phase $\mathcal{L}_{g1}$ is,

$$\frac{\partial f_g}{\partial t} + \nabla_x \cdot \left(\mathbf{u} f_g\right) = \frac{g_g - f_g}{\tau_g}, \tag{41}$$

where $\mathbf{u}$ is the velocity, τ_g is the relaxation time for gas phase, f_g is the distribution function of gas phase, and g_g is the corresponding equilibrium state (Maxwellian distribution). The local equilibrium state g_g can be written as,

$$g_g = \rho_g \left(\frac{\lambda_g}{\pi}\right)^{\frac{K+3}{2}} e^{-\lambda_g\left[(\mathbf{u}-\mathbf{U}_g)^2 + \xi^2\right]},$$

where ρ_g is the density of gas phase, λ_g is determined by gas temperature through $\lambda_g = \frac{m_g}{2k_B T_g}$, m_g is the molecular mass, and $\mathbf{U}_g$ is the macroscopic velocity of gas phase. Here K is the internal degree of freedom with $K = (5-3\gamma)/(\gamma-1)$ for three-dimensional diatomic gas, where $\gamma = 1.4$ is the specific heat ratio. The collision term satisfies the compatibility condition

$$\int \frac{g_g - f_g}{\tau_g} \boldsymbol{\psi} \mathrm{d}\Xi = 0, \tag{42}$$

where $\boldsymbol{\psi} = \left(1, \mathbf{u}, \frac{1}{2}(\mathbf{u}^2 + \boldsymbol{\xi}^2)\right)^T$, the internal variables $\boldsymbol{\xi}^2 = \xi_1^2 + \cdots + \xi_K^2$, and $\mathrm{d}\Xi = \mathrm{d}\mathbf{u}\mathrm{d}\boldsymbol{\xi}$.

For Eq. (41), the integral solution of f at the cell interface can be written as,

$$f(\mathbf{x}, t, \mathbf{u}, \boldsymbol{\xi}) = \frac{1}{\tau}\int_0^t g(\mathbf{x}', t', \mathbf{u}, \boldsymbol{\xi}) e^{-(t-t')/\tau} \mathrm{d}t' \quad + e^{-t/\tau} f_0(\mathbf{x} - \mathbf{u}t, \mathbf{u}, \boldsymbol{\xi}), \tag{43}$$

where $\mathbf{x}' = \mathbf{x} + \mathbf{u}(t' - t)$ is the trajectory of particles, f_0 is the initial gas distribution function at time $t = 0$, and g is the corresponding equilibrium state. The initial NS gas distribution function f_0 in Eq. (43) can be constructed as

$$f_0 = f_0^r(\mathbf{x}, \mathbf{u}) H(x) + f_0^l(\mathbf{x}, \mathbf{u})(1 - H(x)), \tag{44}$$

where $H(x)$ is the Heaviside function, f_0^l and f_0^r are the initial gas distribution functions on the left and right side of one cell interface. More specifically, the initial gas distribution function f_0^k, $k = l, r$, is constructed as

$$f_0^k = g^k\left(1 + \mathbf{a}^k \cdot \mathbf{x} - \tau(\mathbf{a}^k \cdot \mathbf{u} + A^k)\right),$$

where g^l and g^r are the Maxwellian distribution functions on the left and right hand sides of a cell interface, and they can be determined by the corresponding conservative variables $\mathbf{W}^l$ and $\mathbf{W}^r$. The coefficients $\mathbf{a}^l = \left[a_1^l, a_2^l, a_3^l\right]^T$, $\mathbf{a}^r = \left[a_1^r, a_2^r, a_3^r\right]^T$, are related to the spatial derivatives in normal and tangential directions, which can be obtained from the corresponding derivatives of the initial macroscopic variables,

$$\left\langle a_i^l \right\rangle = \partial \mathbf{W}^l / \partial x_i, \left\langle a_i^r \right\rangle = \partial \mathbf{W}^r / \partial x_i,$$

where $i = 1, 2, 3$, and $\langle \ldots \rangle$ means the moments of the Maxwellian distribution functions,

$$\langle \ldots \rangle = \int \boldsymbol{\psi} (\ldots) g \mathrm{d}\Xi.$$

Based on the Chapman–Enskog expansion, the non-equilibrium part of the distribution function satisfies,

$$\left\langle \mathbf{a}^l \cdot \mathbf{u} + A^l \right\rangle = 0, \quad \left\langle \mathbf{a}^r \cdot \mathbf{u} + A^r \right\rangle = 0,$$

and therefore the coefficients A^l and A^r can be fully determined. The equilibrium state g around the cell interface is modeled as,

$$g = g_0\left(1 + \bar{\mathbf{a}} \cdot \mathbf{x} + \bar{A}t\right), \tag{45}$$

where $\bar{\mathbf{a}} = \left[\bar{a}_1, \bar{a}_2, \bar{a}_3\right]^T$, g_0 is the local equilibrium of the cell interface. More specifically, g can be determined by the compatibility condition,

$$\int \boldsymbol{\psi} g_0 \mathrm{d}\Xi = \mathbf{W}_0 = \int_{u>0} \boldsymbol{\psi} g^l \mathrm{d}\Xi + \int_{u<0} \boldsymbol{\psi} g^r \mathrm{d}\Xi,$$

$$\int \boldsymbol{\psi} \bar{a}_i g_0 \mathrm{d}\Xi = \partial \mathbf{W}_0 / \partial x_i = \int_{u>0} \boldsymbol{\psi} a_i^l g^l \mathrm{d}\Xi + \int_{u<0} \boldsymbol{\psi} a_i^r g^r \mathrm{d}\Xi,$$

$i = 1, 2, 3$, and

$$\left\langle \bar{\mathbf{a}} \cdot \mathbf{u} + \bar{A} \right\rangle = 0.$$

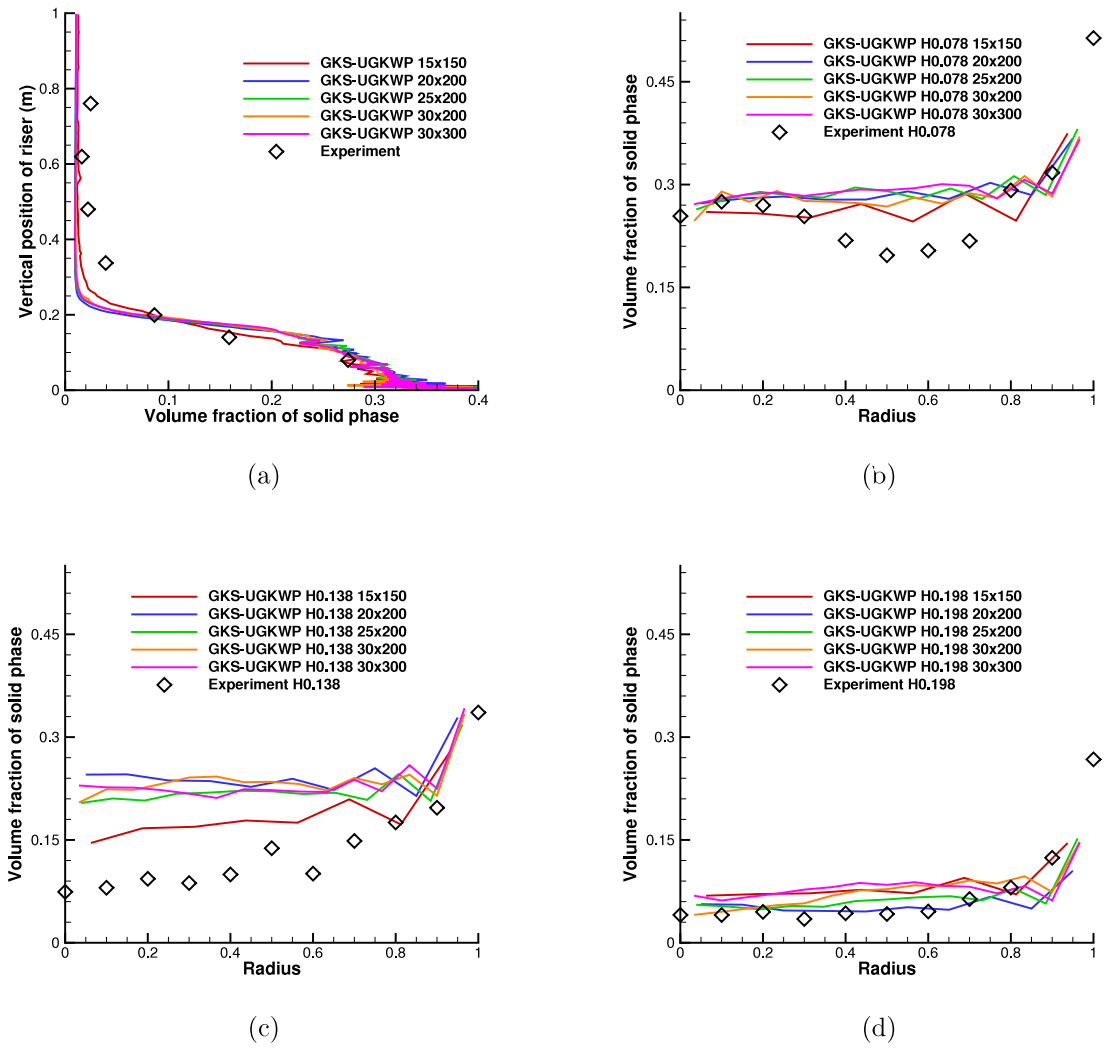

Fig. 2. Time-averaged solid volume fraction ϵ_s with different cell size by GKS-UGKWP in 2D. (a): ϵ_s distribution versus vertical riser height. (b–d): ϵ_s distribution versus horizontal radius at three different heights, 0.078 m, 0.138 m, and 0.198 m.

After determining all parameters in the initial gas distribution function f_0 and the equilibrium state g, substituting Eqs. (44) and (45) into Eq. (43), the time-dependent distribution function $f(\mathbf{x}, t, \mathbf{u}, \boldsymbol{\xi})$ at a cell interface can be expressed as,

$$\begin{aligned} f(\mathbf{x}, t, \mathbf{u}, \boldsymbol{\xi}) = {} & c_1 g_0 + c_2 \bar{\mathbf{a}} \cdot \mathbf{u} g_0 + c_3 \bar{A} g_0 \\ & + \left[c_4 g^r + c_5 \mathbf{a}^r \cdot \mathbf{u} g^r + c_6 A^r g^r \right] (1 - H(u)) \\ & + \left[c_4 g^l + c_5 \mathbf{a}^l \cdot \mathbf{u} g^l + c_6 A^l g^l \right] H(u). \end{aligned} \tag{46}$$

with coefficients,

$$\begin{aligned} c_1 &= 1 - e^{-t/\tau}, \\ c_2 &= (t + \tau) e^{-t/\tau} - \tau, \\ c_3 &= t - \tau + \tau e^{-t/\tau}, \\ c_4 &= e^{-t/\tau}, \\ c_5 &= -(t + \tau) e^{-t/\tau}, \\ c_6 &= -\tau e^{-t/\tau}. \end{aligned}$$

Then, the integrated flux over a time step can be obtained,

$$\mathbf{F}_{ij} = \int_0^{\Delta t} \int \mathbf{u} \cdot \mathbf{n}_{ij} f_{ij}(\mathbf{x}, t, \mathbf{u}, \boldsymbol{\xi}) \boldsymbol{\psi} \mathrm{d}\Xi \mathrm{d}t, \tag{47}$$

where $\mathbf{n}_{ij}$ is the normal vector of the cell interface. Then, the cell-averaged conservative variables of cell i can be updated as follows,

$$\mathbf{W}_i^{n+1} = \mathbf{W}_i^n - \frac{1}{\Omega_i} \sum_{S_{ij} \in \partial\Omega_i} \mathbf{F}_{ij} S_{ij}, \tag{48}$$

where Ω_i is the volume of cell i, $\partial\Omega_i$ denotes the set of interface of cell i, S_{ij} is the area of jth interface of cell i, $\mathbf{F}_{ij}$ denotes the projected macroscopic fluxes in the normal direction, and $\mathbf{W}_g = \left[\rho_g, \rho_g \mathbf{U}_g, \rho_g E_g\right]^T$ are the cell-averaged conservative flow variables for gas phase. Now the update of the first part $\mathcal{L}_{g1}$ has been finished.

The second part, $\mathcal{L}_{g2}$, is from the inter-phase interaction. The increased macroscopic variables for gas phase in 3D can be calculated as

$$\mathbf{W}_g^{n+1} = \mathbf{W}_g + \mathbf{Q} \Delta t, \tag{49}$$

where

$$\mathbf{W}_g = \begin{bmatrix} \rho_g \\ \rho_g \mathbf{U}_g \\ \rho_g E_g \end{bmatrix},$$

$$\mathbf{Q} = \begin{bmatrix} C_{\epsilon_g} \rho_g \\ C_{\epsilon_g} \rho_g \mathbf{U}_g - \frac{\epsilon_s \rho_s (\mathbf{U}_g - \mathbf{U}_s)}{\epsilon_g \tau_{st}} + \frac{\rho_g \mathbf{G}}{\epsilon_g} \\ C_{\epsilon_g} \left(\rho_g E_g + p_g\right) - \frac{\epsilon_s \rho_s \mathbf{U}_s \cdot (\mathbf{U}_g - \mathbf{U}_s)}{\epsilon_g \tau_{st}} + \frac{3 p_s}{\epsilon_g \tau_{st}} + \frac{\rho_g \mathbf{U}_g \cdot \mathbf{G}}{\epsilon_g} \end{bmatrix}.$$

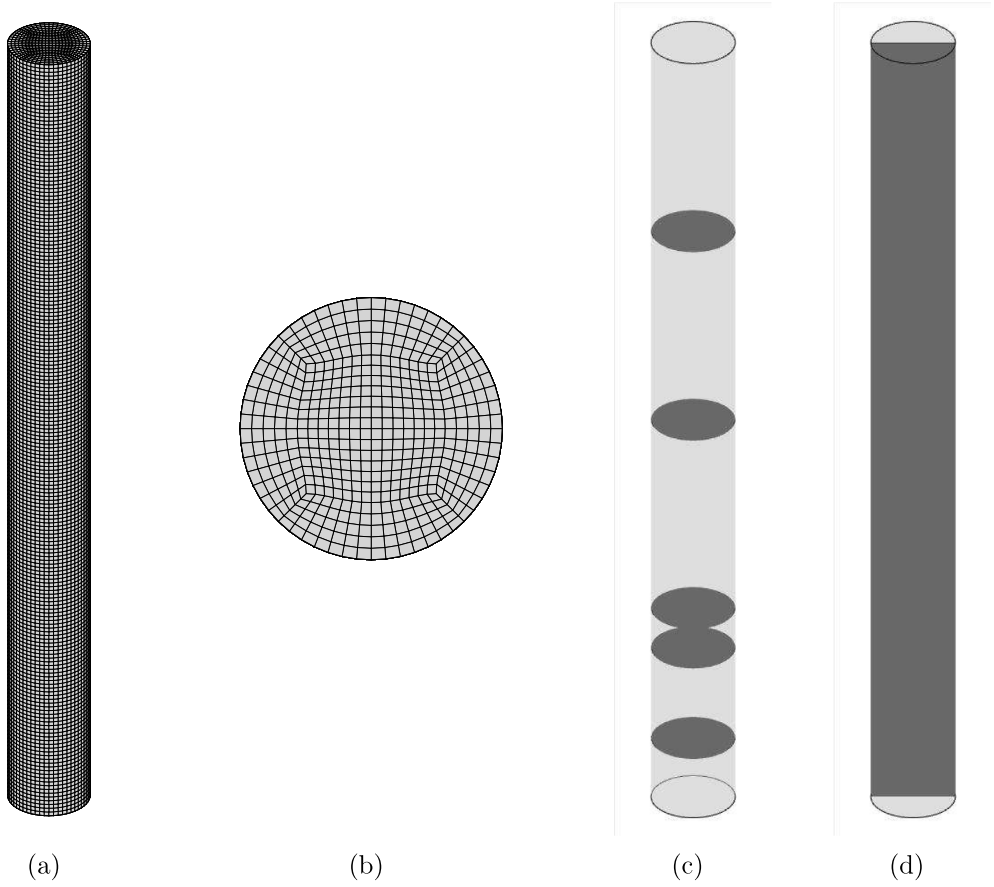

Fig. 3. Sketch of mesh and cross section used in post-processing: (a) the mesh employed in 3D view, (b) the mesh with 476 cells in one 2D cross section, (c) the horizontal cross sections at heights 0.078 m, 0.198 m, 0.25 m, 0.50 m and 0.75 m, where the flow distributions will be shown at these cross sections later, and (d) the vertical cross section.

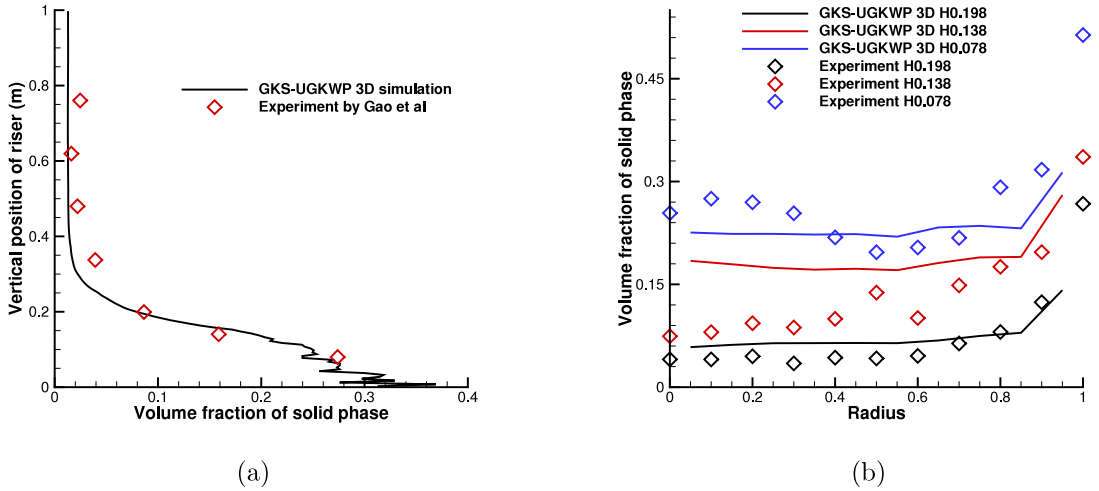

Fig. 4. Time-averaged solid volume fraction ϵ_s and the comparison with experimental measurement. (a): ϵ_s distribution versus vertical riser height. (b): ϵ_s distribution versus horizontal radius at three different heights, 0.078 m, 0.138 m, and 0.198 m.

Note that the $\mathbf{W}_g$ are the macroscopic variables after updating $\mathcal{L}_{g1}$ as described before. In Q, the term $C_{\epsilon_g}\mathbf{W}_g$ is caused by the nozzle term and pDV work term in Eq. (37). Here C_{ϵ_g} is given by $C_{\epsilon_g} = -\frac{1}{\epsilon_g}\frac{\mathrm{d}\epsilon_g}{\mathrm{d}t}$ with $\frac{\mathrm{d}\epsilon_g}{\mathrm{d}t} = \frac{\partial\epsilon_g}{\partial t} + \mathbf{U}_g \cdot \nabla\epsilon_g$. In this paper, $\frac{\partial\epsilon_g}{\partial t}$ is evaluated as,

$$\frac{\partial \epsilon_g}{\partial t} = \frac{\epsilon_g^{n+1} - \epsilon_g^n}{\Delta t}. \tag{50}$$

Here $\nabla\epsilon_g$ is the cell-averaged volume fraction gradient of gas phase in the cell. For example, $\frac{\partial\epsilon_g}{\partial x}$ is calculated by,

$$\frac{\partial \epsilon_{g,i}}{\partial x} = \frac{\epsilon_{g,i+\frac{1}{2}} - \epsilon_{g,i-\frac{1}{2}}}{\Delta x}, \tag{51}$$

where $\epsilon_{g,i-\frac{1}{2}}$ and $\epsilon_{g,i+\frac{1}{2}}$ are volume fractions of gas phase at the left and right interface of cell i, which can be obtained from the reconstructed ϵ_s according to $\epsilon_s + \epsilon_g = 1$. Note that the gravity $\mathbf{G}$ of gas phase is

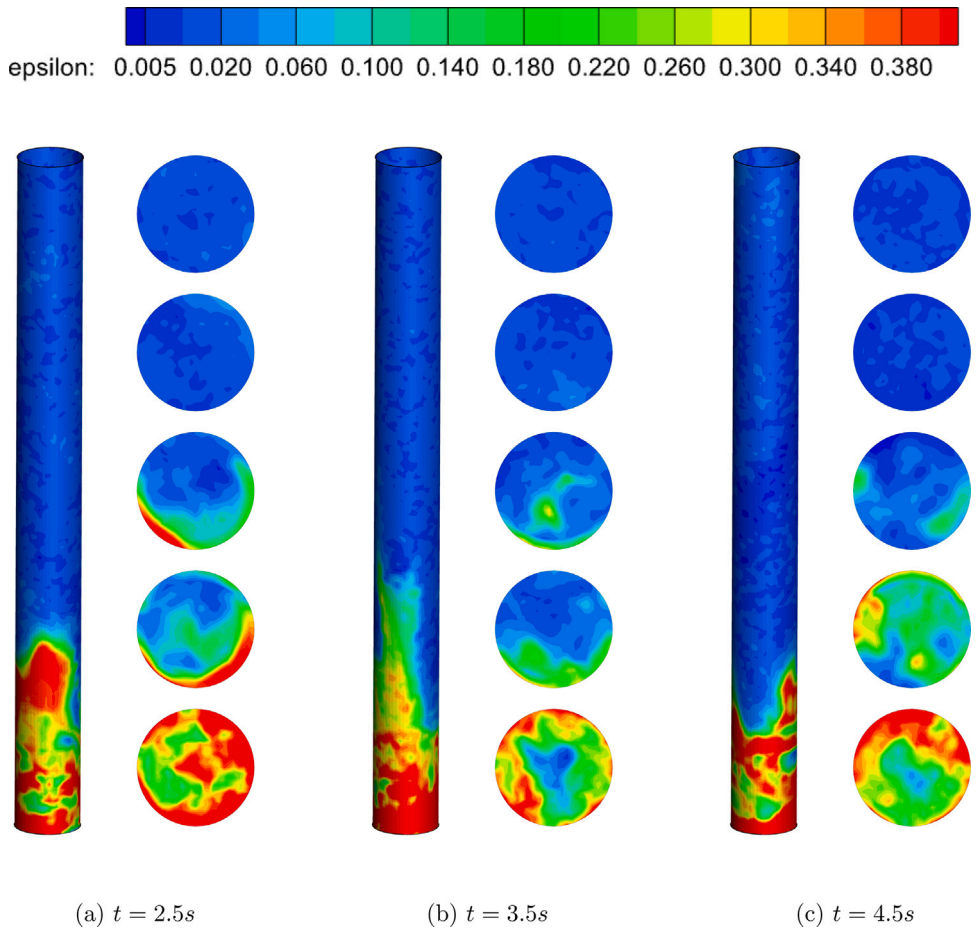

Fig. 5. Instantaneous snapshots of solid volume fraction ϵ_s by GKS-UGKWP at different times: (a) $t = 2.5$ s, (b) $t = 3.5$ s, (c) $t = 4.5$ s. ϵ_s distributions near the surface of cylinder wall and at the horizontal cross sections at heights 0.078 m, 0.198 m, 0.25 m, 0.50 m and 0.75 m, see Fig. 3(c), are presented.

ignored in this paper. Now the update for the gas phase in one time step has been finished.

Finally, the algorithm of GKS-UGKWP method for the gas-particle flow is summarized in Fig. 1.

4. Numerical experiments

In the following cases, the time step of gas phase Δt_g is determined by,

$$\Delta t_g = \mathrm{CFL} \times \left[\frac{\Delta_c}{\mathbf{U}_g + \sqrt{\gamma R T_g}} \right]_{\min},$$

where Δ_c is the cell size. Similarly, the time step of solid phase Δt_s is determined by

$$\Delta t_s = \mathrm{CFL} \times \left[\frac{\Delta_c}{\mathbf{U}_s + a\sqrt{\theta}} \right]_{\min},$$

where a is taken as 3, and CFL is taken as 0.5 in this paper. For most fluidized bed problems, Δt_s is larger than Δt_g, more than one order. Therefore, in this paper, two time steps Δt_s and Δt_g are used in the evolution of solid and gas phase, respectively; since $\Delta t_s > \Delta t_g$, the solid phase will be frozen when the gas phase is evolved by Δt_g.

4.1. Turbulent fluidized bed problem

4.1.1. Case description

The first case is a turbulent fluidized bed problem studied experimentally by Gao et al. [40]. This experiment was conducted on a fluidized system, including a fluidizing column, an expanded column, and a recycling system. In this paper, only the fluidizing column is simulated, as the previous study by CFD model [40]. The computational domain is a three-dimensional cylinder with diameter $D = 0.095$ m and height $H = 1$ m. The material density and diameter of solid particles are $\rho_s = 2400\ \mathrm{kg}/m^3$ and $d = 0.139$ mm, and the maximum solid volume fraction $\epsilon_{s,max}$ is 0.63. In this paper, the case with initial bed height $H_0 = 0.096$ m and inlet gas velocity $U_g = 1.25$ m/s is calculated by GKS-UGKWP. Initially the equivalent solid mass is uniformly distributed in the computational domain; in the simulation, the solid particles are free to leave at the top boundary, and the escaped solid mass is recirculated to the computational domain through the bottom boundary to maintain a constant solid inventory in the riser. The gas blows into the fluidized bed with a uniform vertical velocity U_g and a pressure $\Delta p = \epsilon_{s,max}\left(\rho_s - \rho_g\right) G H_0$. The non-slip wall and slip wall boundary condition are employed for gas phase and solid phase respectively for the riser wall. For the turbulent fluidized bed, the particle distributions composed of dense bottom, transition middle, and dilute top zone are commonly observed in the previous numerical and experimental studies. Therefore, the drag model proposed by Gao et al. [40] in all aforementioned zones is employed in this turbulent fluidized bed study,

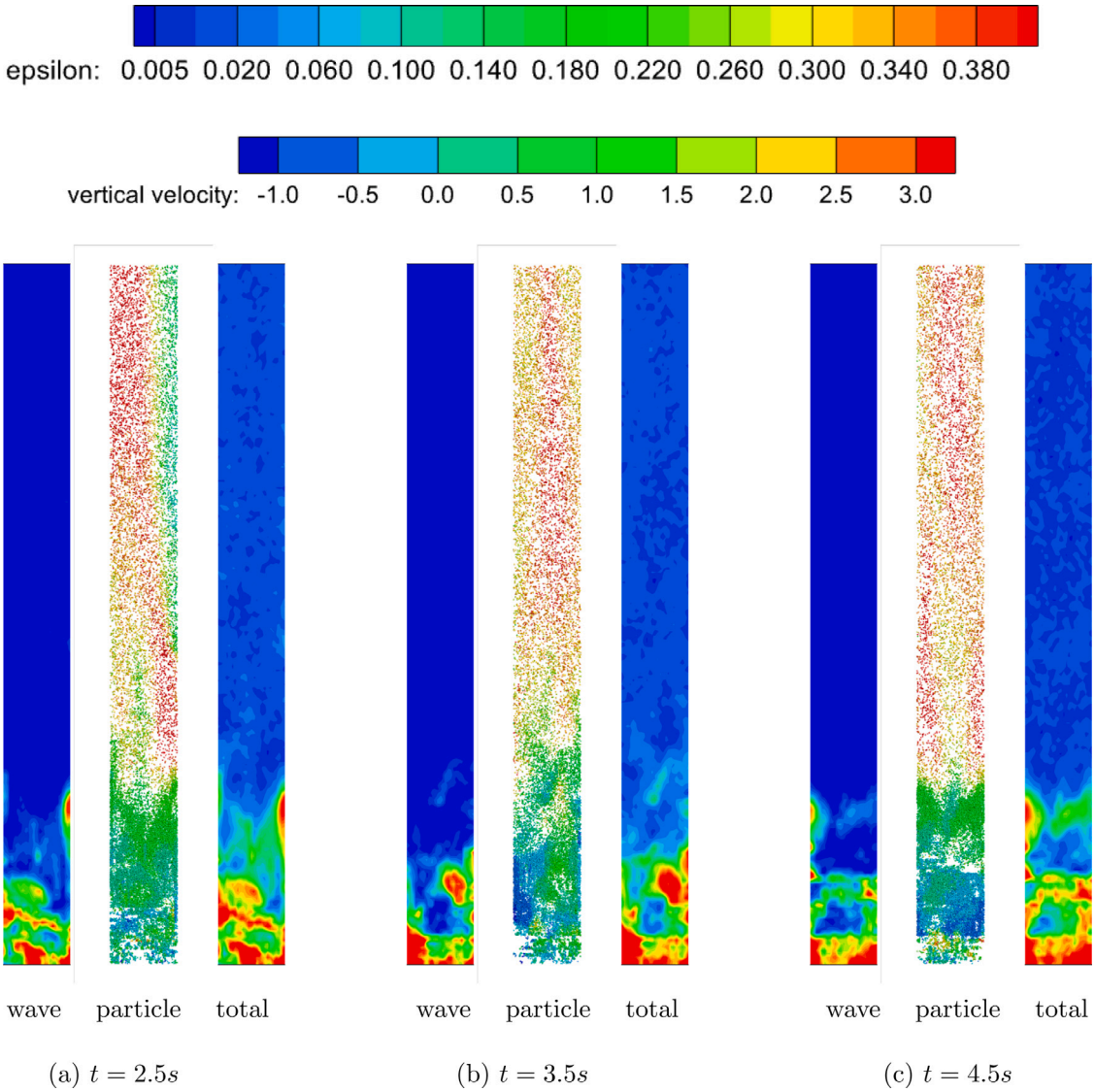

Fig. 6. Solid volume fraction ϵ_s represented by wave and discrete particle (colored by vertical velocity) at different times: (a) $t = 2.5$ s, (b) $t = 3.5$ s, (c) $t = 4.5$ s, on the vertical symmetric cross-section shown in Fig. 3(d). The sub-figures give the individual **wave** and **particle** decomposition, and the **total** ϵ. The **wave** composition (ϵ_s^{wave}) is colored by the epsilon-legend. The discrete **particle** composition is colored by the vertical velocity-legend. The **total** ϵ_s is also colored by the epsilon-legend. Note that ϵ_s is exactly the sum of wave and discrete particle decomposition, such as **wave** + **particle** = **total**.

and the inter-phase momentum transfer coefficient β in this drag model can be written as follows,

$$\beta = \begin{cases} 0.001\left(\dfrac{17.3}{Re_s} + 0.336\right)\dfrac{\rho_g|\mathbf{U}_g - \mathbf{u}|}{d_s}\epsilon_s\epsilon_g^{-1.8}, & \epsilon_g \le 0.94, \\ \dfrac{3}{4}C_d\dfrac{\rho_g\epsilon_s\epsilon_g|\mathbf{U}_g - \mathbf{u}|}{d_s}\epsilon_g^{-2.65}, & 0.94 < \epsilon_g \le 0.99, \\ \dfrac{3}{4}C_d\dfrac{\rho_g\epsilon_g|\mathbf{U}_g - \mathbf{u}|}{d_s}, & 0.99 < \epsilon_g \le 1.0, \end{cases} \tag{52}$$

where $Re_s = \epsilon_g|\mathbf{U}_g - \mathbf{u}|d_s/\nu_g$ is the particle Reynolds number, ν_g is the kinematic viscosity of gas phase, and C_d is the Re_s dependent drag coefficient,

$$C_d = \begin{cases} \dfrac{24}{Re_s}\left(1 + 0.15Re_s^{0.687}\right), & Re_s \le 1000, \\ 0.44, & Re_s > 1000. \end{cases} \tag{53}$$

4.1.2. Results

To determine the cell size effect, the two-dimensional simulations in a computational domain 0.095 m × 1 m with different cell numbers are conducted firstly. Specifically, the uniform rectangular mesh with cell numbers 15 × 150, 20 × 200, 25 × 200, 30 × 200, and 30 × 300, are calculated by GKS-UGKWP, respectively. Fig. 2 presents the time-averaged distribution of solid volume fraction ϵ_s vertically and radially at different riser heights, 0.078 m, 0.138 m, and 0.198 m. The results indicate that except for very coarse mesh 15 × 150, other cases give very similar prediction. Therefore, the mesh sizes with 24 cells in the diameter D and 200 cells in the riser height H are employed for three-dimensional simulation, as shown in Fig. 3. In particular, the mesh cells are hexahedrons with a total number of 95200 control volumes, composed of a horizontal 476 cells with 200 layers in the vertical direction, where the cells are nearly uniformly distributed in the whole domain.

The time-averaged solid volume fraction ϵ_s in three-dimensional simulation during time 2.0 s ~ 5.5 s is shown in Fig. 4, and the experimental measurement results are also presented for comparison. Overall, the profiles of ϵ_s along with the riser height and the radius agree well with the experiment measurement. In the current study, an accurate drag model is employed to reflect the phase-interaction for accurate capturing of the profile ϵ_s in the vertical direction. However,

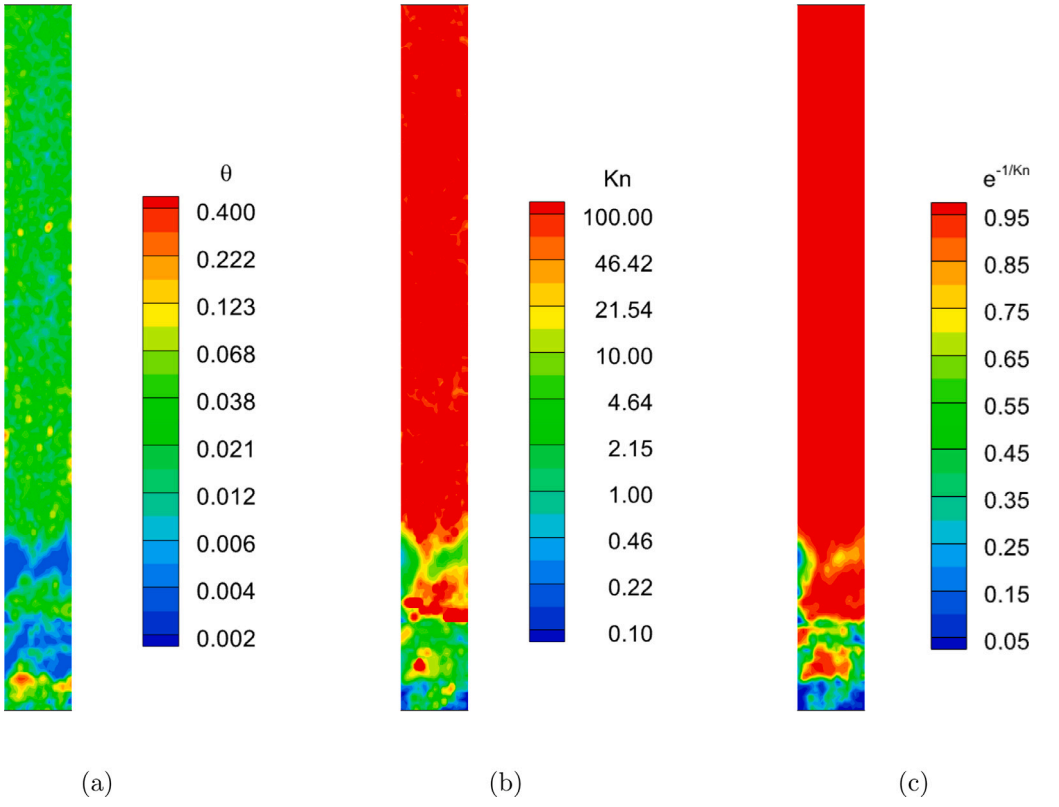

Fig. 7. The instantaneous snapshots of: (a) granular temperature θ, (b) Kn, (c) $e^{-1/\mathrm{Kn}}$, at $t = 4.5$ s on the vertical symmetric cross-section shown in Fig. 3(d). The legend of θ and Kn are in exponential distribution.

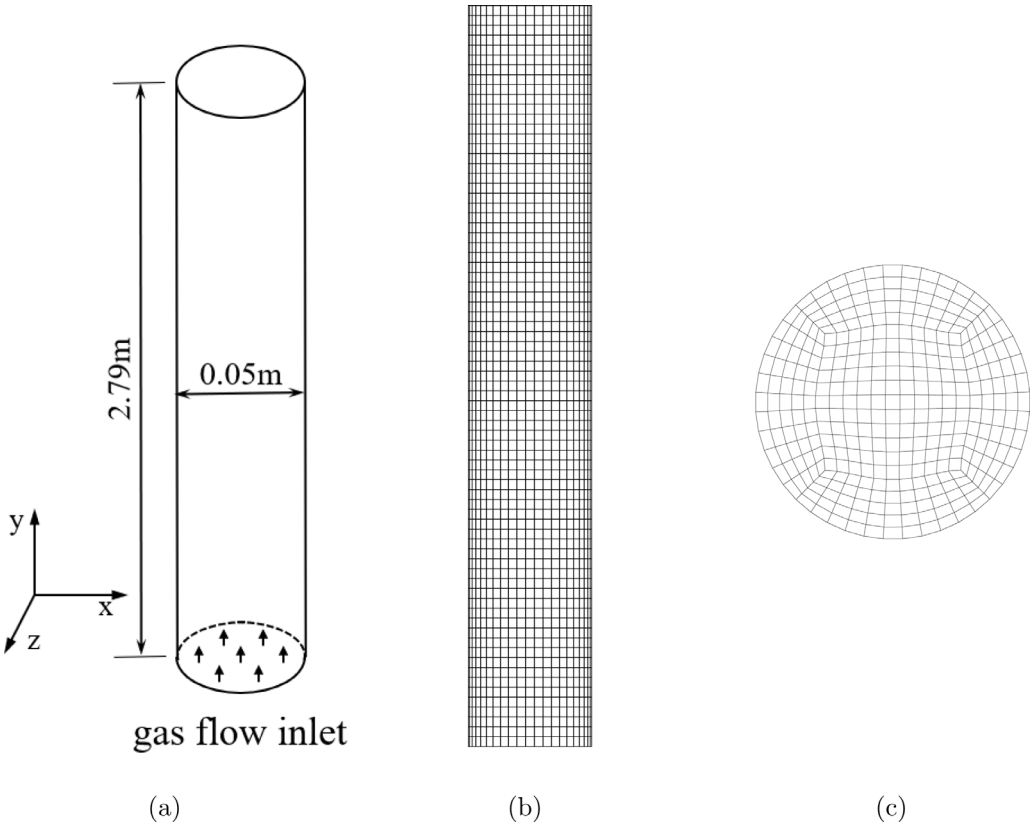

Fig. 8. Sketch of geometry and mesh of Horio riser: (a) geometry of the riser employed in this paper, (b) the mesh from the front view (with a section of 0.3 m in height), (c) the mesh on each cross-section.

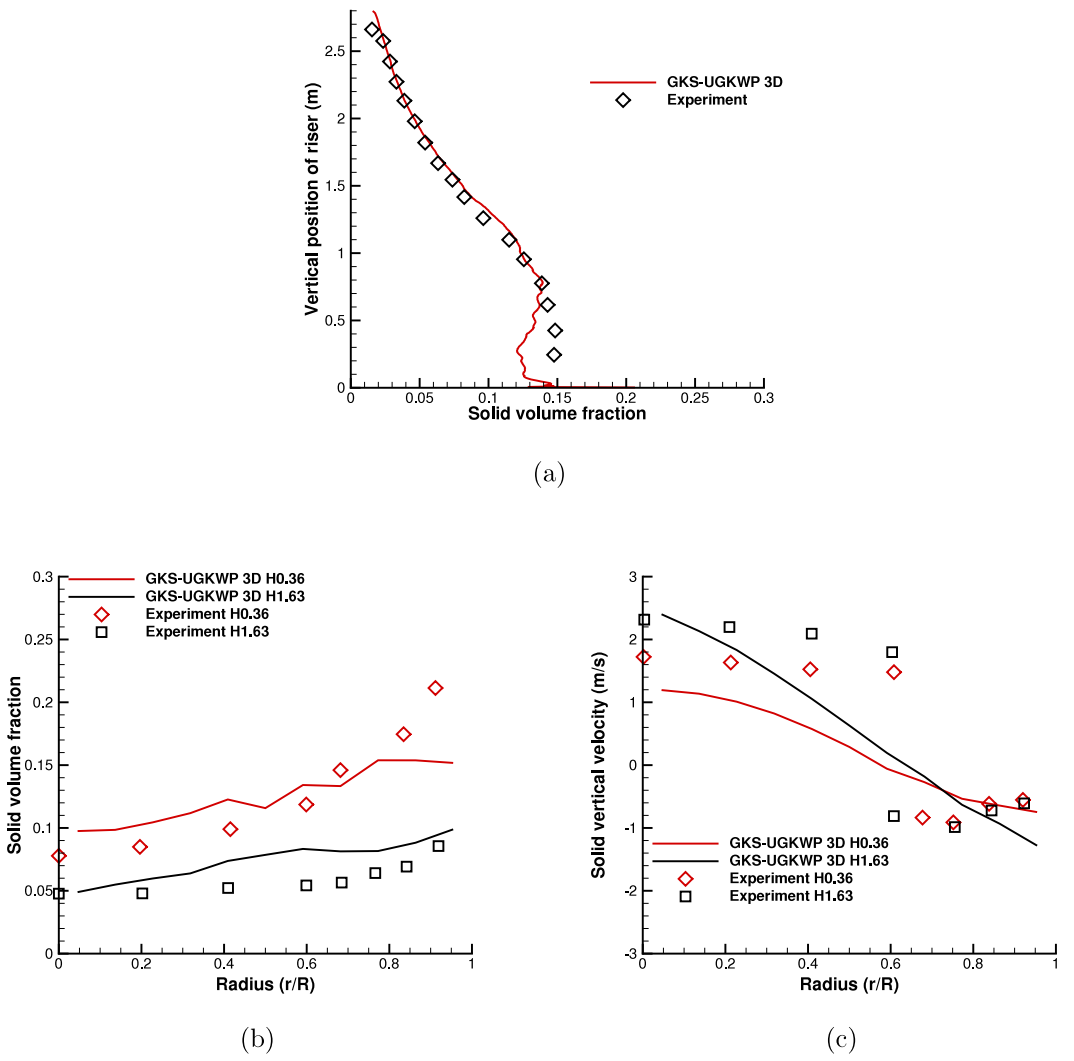

Fig. 9. Time-averaged volume fraction ϵ_s and vertical velocity V_s of solid phase from GKS-UGKWP and experiment measurement: (a) ϵ_s distribution along the riser height, (b) ϵ_s distribution along the riser radius at 0.36 m and 1.63 m respectively, (c) V_s distribution along the riser radius at 0.36 m and 1.63 m respectively.

as shown in Fig. 4(b), the presented ϵ_s near the wall by GKS-UGKWP is lower than the experiment measurement at all three heights, where more accurate model for the near-wall zone has to be developed. Fig. 5 presents the instantaneous snapshots of solid volume fraction ϵ_s at times 2.5 s, 3.5 s, and 4.5 s. The distributions of ϵ_s at different horizontal cross-sections, at the locations in Fig. 3(c), are shown. The results show the solid particle dense region (bottom), transition region (middle), and dilute region (top). Besides, the radial heterogeneous structure of solid particles can be found in the horizontal cross-sections. In general, the solid particles concentrate in the near-wall region. These typical flow features are also observed in the previous experimental and numerical simulation [40]. Overall, GKS-UGKWP can give a reasonable prediction for this fluidized bed problem.

In order to show the coupled evolution of wave and particle in UGKWP for solid particle flow, the constitution of wave and sampled particle at different times are shown in Fig. 6. More specifically, the distributions from the decompositions of wave and discrete particle are clearly presented by “wave" and “particle", of which the sum is exactly the total ϵ_s. As described before, in UGKWP the weights of mass distribution is based on the local Kn by $(1-\exp(-1/\mathrm{Kn}))$ for wave decomposition and $\exp(-1/\mathrm{Kn})$ for discrete particle decomposition. The instantaneous distribution of local Kn and the value of $\exp(-1/\mathrm{Kn})$ at $t = 4.5$ s, corresponding to Fig. 6(c), are presented in Fig. 7(b) and Fig. 7(c), respectively. Here Kn is determined by τ_s/t_{ref} with τ_s defined in Eq. (30), which depends on the solid volume fraction ϵ_s, shown in Fig. 6(c) marked by “total”, and granular temperature θ, shown in Fig. 7(a). The characteristic time t_{tef} is the time step of solid phase Δt_s. The results show that for this turbulent fluidized bed, the solid phase is generally dilute in the riser’s top region (above 0.3 m in height), where the particle free transport is dominant with a large Kn, and the particle phase is in a non-equilibrium state driven by the gas flow. On the other hand, in the bottom region the particles are highly concentrated with a small Kn, especially in the zones near riser wall. In this region, the intensive particle–particle collision pushes the particle distribution to an equilibrium state, and the particle phase evolution is mainly controlled by the wave component through the hydrodynamic flow variables. As a result, in UGKWP few particles will appear in this region, even though abundant solid particles exist here. Besides the above limiting cases, in the transition regions with an intermediate Kn, such as the layers with height between $0.1\ m \sim 0.2$ m, both wave and discrete particle influence the evolution and the solution update through the fluxes in Eq. (22), where both hydrodynamic wave (EE)

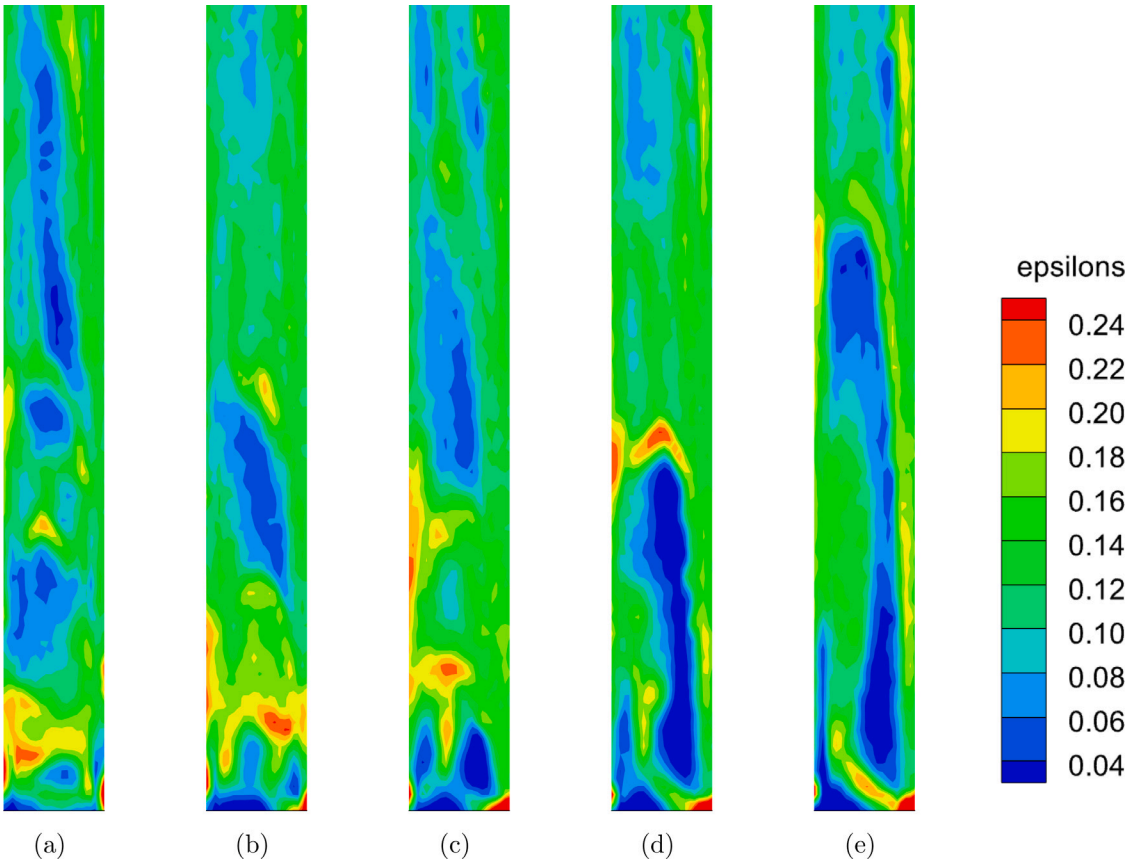

Fig. 10. Instantaneous snapshots of solid volume fraction ϵ_s on the vertical symmetric plane in a zone with heights from 0 to 0.4 m at different times: (a) $t = 7.0$ s, (b) $t = 7.1$ s, (c) $t = 7.2$ s, (d) $t = 7.3$ s, (e) $t = 7.4$ s.

and discrete particles transport (EL) have contributions. The modeling in UGKWP captures the multi-scale nature of solid particle transport and presents a smooth transition to cover the dense, transition, and dilute particle regions in a fluidized bed.

4.2. Circulating fluidized bed case

4.2.1. Case description

In the following, the 3D circulating fluidized bed of Horio et al. is simulated by GKS-UGKWP [50]. This case has been taken as a typical example to validate the numerical methods for gas-particle two-phase flow [49,61]. The sketch of the riser is shown in Fig. 8(a), and the computational domain is a cylinder with a diameter $D = 0.05$ m and a height $H = 2.80$ m, which is 0.01 m higher than the actual size. The numerical cells are hexahedron. Fig. 8(b) and Fig. 8(c) present the mesh from the front (a section of 0.3 m in height) and top view, respectively. The total number of cells is 238700 with 341 in horizontal surface and 700 in the vertical direction. The cell size is approximately $\Delta = 2.26 \times 10^{-3}$ m horizontally and $\Delta = 4.00 \times 10^{-3}$ m vertically. For the circulating fluidized bed, the semi-empirical model proposed by Pallares can be used to approximately estimate the wall-layer thickness t_{wall}, which is defined as the distance form the wall to the position of zero local solid flux in vertical direction [62]. In this case the wall-layer thickness according to Pallares' model is $t_{wall} = 0.0648D = 3.24\times10^{-3}$ m; and further the near-wall cell size in this paper is around $\Delta_{wall} = 2.24\times10^{-3}$ m, smaller than the size of estimated t_{wall}. The solid particles employed in the experiment have material density $\rho_s = 1000$ kg/m^3 and diameter $d_s = 60$ um. In the numerical simulation, initially the solid particles are uniformly distributed in the whole riser with a solid volume fraction $\epsilon_{s,0} = 0.086$. For the gas phase, the top boundary is set as the outlet pressure, and the air blows from the bottom into the riser with the uniform velocity $U_g = 1.17$ m/s and pressure $\epsilon_{s,0}\left(\rho_s - \rho_g\right)GH$. Same as the previous case, solid particles can escape from the riser at the top boundary, and come back into the riser at the bottom boundary, ensuring a constant solid material in the riser. At the cylinder surface, the non-slip wall boundary condition is used for the gas phase; while for the solid phase, the mixed boundary condition proposed by Johnson et al. is employed [56].

The MP-PIC method coupled with EMMS drag force was employed to study this case, and the results showed obvious improvement than the traditional homogeneous drag model proposed by Gidaspow [49]. In the current study, the EMMS drag force model is used in GKS-UGKWP method for this circulating fluidized bed riser,

$$\beta = \frac{3}{4}C_d\frac{\rho_g\epsilon_s\epsilon_g|\mathbf{U}_g - \mathbf{u}|}{d_s}\epsilon_g^{-2.7}H_D, \tag{54}$$

where Re_s is the particle Reynolds number, and C_d is the drag coefficient calculated by Eq. (53). The H_D is the so-called heterogeneity index, which is defined as,

$$H_D = a\left(Re_s + b\right)^c, \tag{55}$$

and a, b, and c are the model parameters dependent on the solid volume fraction ϵ_s and with the consideration of local heterogeneous flow structures. The specific values of model parameters (a, b, c) are listed in Appendix A, and more detailed introduction about EMMS drag force can refer to the previous work [48,49].

4.2.2. Results

The time-averaged distributions of solid particles and the vertical solid velocity from the time interval 4.0 s ~ 7.5 s are shown in Fig. 9. Fig. 9(a) presents the profile of ϵ_s along with the riser height, which covers heterogeneous feature of the solid flow from bottom dense

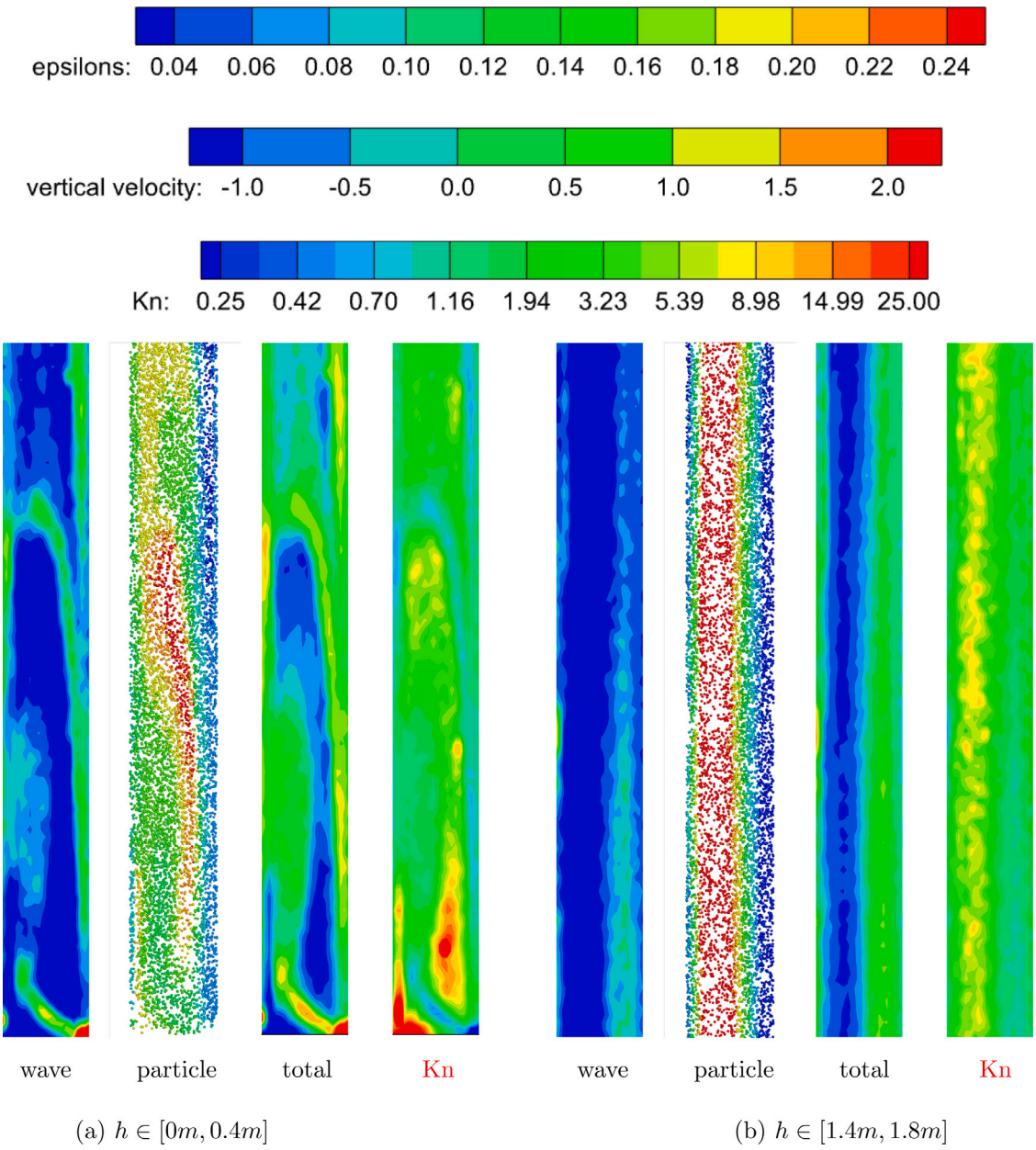

Fig. 11. The instantaneous snapshots of the solid volume fraction ϵ_s of wave decomposition and discrete particles, and Kn at $t = 7.4$ s in different vertical zones: (a) $h \in [0\text{ m}, 0.4\text{ m}]$, (b) $h \in [1.4\text{ m}, 1.8\text{ m}]$. The sub-figures shown from left to right give the individual **wave** and **particle** decomposition, the **total** ϵ, and the Kn. The **wave** composition (ϵ_s^{wave}) is colored by the epsilon-legend. The discrete **particle** composition is colored by the vertical velocity-legend. The **total** ϵ_s is also colored by the epsilon-legend. The Kn is colored by the Kn-legend. Note that ϵ_s is exactly the sum of wave and discrete particle decomposition, such as **wave** + **particle** = **total**.

region, across middle transition region, and up to the top dilute region. This flow feature is similar to that in the turbulent fluidized bed. However, in the circulating fluidized bed, the transition between dense and dilute regions is moderate, as shown in Fig. 4(a) and Fig. 9(a). Although a slight deviation exists at the bottom region (below 0.5 m), the vertical S-shaped curve of ϵ_s is captured by GKS-UGKWP for this circulating fluidized bed problem, and it agrees with the experimental measurement very well. It may come from accurate inter-phase interaction EMMS drag model. The time-averaged distribution of solid volume fraction ϵ_s and solid vertical velocity V_s along the riser radius at height 0.36 m and 1.63 m are shown in Fig. 9(b) and Fig. 9(c), respectively. At both bottom region at height 0.36 m and top region at height 1.63 m, the solid particles show higher concentration in the near-wall region than that in the central region. At the same time, the solid particle vertical velocity shows the upward movement in the central region and downward motion in the near-wall region. This so-called core-annular flow structure is widely observed in the circulating fluidized bed riser. The obtained ϵ_s and V_s by GKS-UGKWP agree well with the experiment data, and the deviations deserve further investigation.

Several instantaneous snapshots of solid volume fraction ϵ_s at a few times in the interval $7.0s \sim 7.4$ s are shown in Fig. 10. Here the results are shown at the bottom region with height below 0.4 m on the symmetric plane. The particle concentrating clusters and diluting bubbles form, move, and vanish dynamically, which may introduce challenges for the hybrid EE and EL numerical methods in identifying the interface between dilute/dense regions. For UGKWP, the wave and particle decompositions are automatically distributed according to the local cell's Kn, where particle appears in tracking the non-equilibrium dilute region, and vanishes in the intensive collisional dense region. At $t = 7.4$ s, the wave and discrete particle decompositions on the

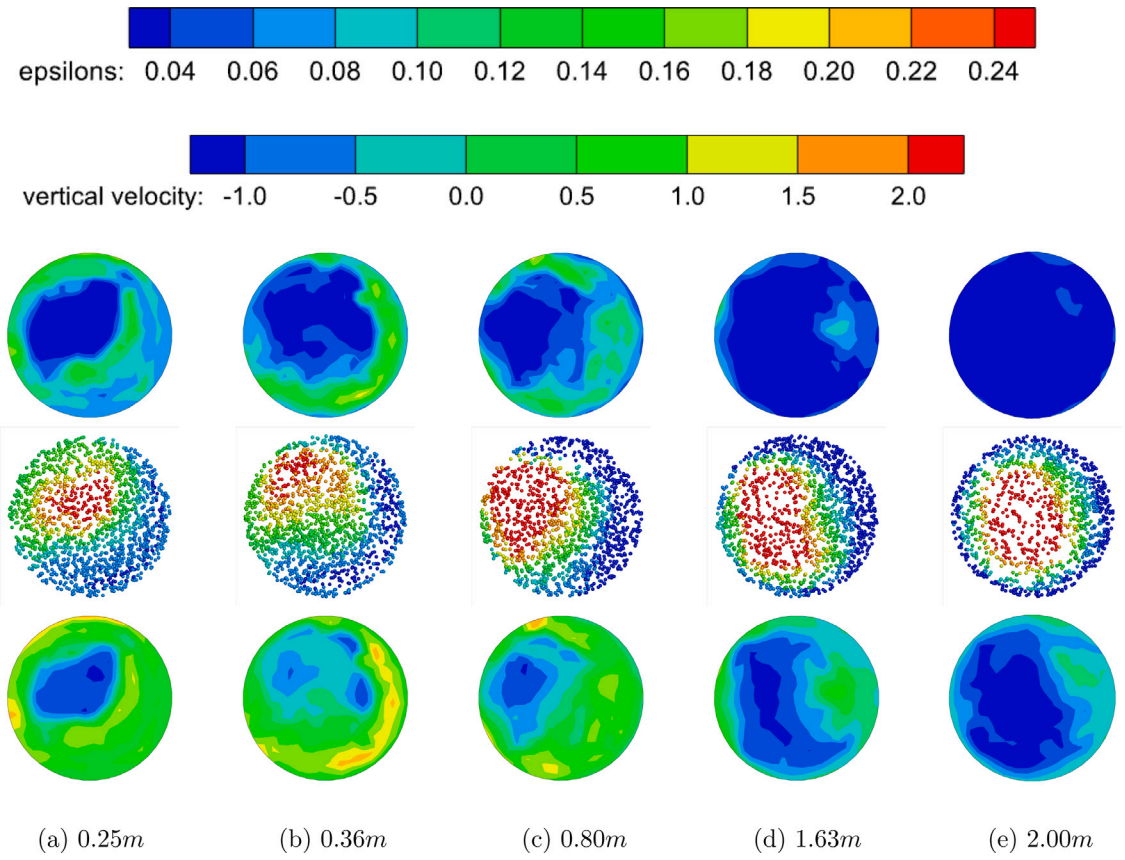

Fig. 12. Solid volume fraction ϵ_s of wave decomposition and discrete particles at t = 7.4 s at different heights: (a) 0.25 m, (b) 0.36 m, (c) 0.80 m, (d) 1.63 m, (e) 2.00 m. At each height of (a) ~ (e), three pictures shown from up to down are: **wave**, **particle**, **total**. **wave** and **total** are colored by epsilons-legend, and **particle** is colored by vertical velocity-legend. ϵ_s in **total** is exactly the sum of **wave** and **particle**.

symmetric plane at regions 0 ~ 0.4 m and 1.4 ~ 1.8 m, and on the horizontal cross-sections at heights, 0.25 m, 0.36 m, 0.80 m, 1.63 m, 2.00 m, are presented in Fig. 11 and Fig. 12, respectively. The sampled particles, shown in Figs. 11 and 12, are colored by their vertical velocity. Furthermore, the local cell's Kn, which is calculated by ratio of the solid particles' collision time τ_s over the time step of solid phase Δt_s, is also shown in Fig. 11, and it determines the percentages of wave and particle component in the solid particle volume fraction. These results clearly show the evolution of solid particle phase through hydrodynamic wave and discrete particle and smooth transition in different regions. The typical core-annular structures are clearly shown from the time-averaged variables in Fig. 9, and the instantaneous snapshots in Fig. 11, and Fig. 12. Particularly, Fig. 12 presents that, the central zone is in a low concentration (ϵ_s < 0.1) solid particle region, with high vertical velocity (V_s > 1.0 m/s). While in the near-wall zone, the solid vertical velocity is usually negative, which indicates that the solid particles move upward in the center region, gather and fall down in the near-wall region. The simulation results validate the GKS-UGKWP method for the study of gas–solid circulating fluidized bed problem.

Another interesting observation is that the experiment shows a very sharp jump in the solid particle vertical velocity around r/R = 0.6 position and height 1.63 m, with a velocity change from 1.8 m/s to −0.8 m/s, as shown in Fig. 9(c). It indicates the highly non-equilibrium transition layer in the solid phase. In practice, UGKWP is capable of capturing the strong non-equilibrium physics, such as keeping a bimodal distribution in the particle velocity distribution function, such as the verification in the problem of two impinging particle jets [24]. In addition, the stratified flow structure, shown in Fig. 11(b), is most likely the flow pattern associated with such a sharp velocity jump observed in the experiment.

5. Conclusion

In this paper, the gas–solid particle two phase flows, i.e., the turbulent fluidized bed and the circulating fluidized bed, are simulated by a 3D multiscale GKS-UGKWP method with coupled wave propagation and particle tracking in the evolution. For the turbulent fluidized bed, the bottom dense/middle transition/top dilute regions coexist and are dynamically interconvertible. This characteristic flow pattern brings great challenges for the single scale methods and the hybrid EE/EL method. To capture such a complex multiscale flow pattern smoothly, UGKWP has the advantages because of its automatic decomposition of wave and particle representation according to the local cell's Knudsen number Kn. At the top dilute regions with a large Kn, the free transport of solid particle is dominant and UGKWP will track the evolution of individual particle. On the other hand, at the bottom region with a small Kn, the particle is highly concentrated with intensive particle–particle collision. The velocity distribution function of the solid particle phase will get close to the Maxwellian distribution. As a result, the evolution of solid phase in this region is mainly determined by the wave evolution, i.e, the so-called two fluid model approach for the gas–solid particle system, even though tremendous amount of real particles exist. Finally, in the transition region with a variable Kn, both wave and particle decompositions contribute to the dynamic evolution of the particle phase. UGKWP will automatically find the most efficient way through the distribution of wave and particle in order to capture accurate flow physics and keep efficient numerical computation. For the circulating fluidized bed of Horio, the particle clusters and dilute bubbles form, move, and vanish dynamically at the bottom region of the riser. Furthermore, the core-annular flow structures, such that the solid particles move upward with a low concentration in the center

Table 1
Parameters in EMMS drag model.

$\begin{cases} a = 0.8526 - \frac{0.5846}{1+(\epsilon_g/0.4325)^{22.6279}} \\ c = 0 \end{cases}$	$0.4 \le \epsilon_g < 0.46$
$\begin{cases} a = 0.0320 + \frac{0.7399}{1+(\epsilon_g/0.4912)^{54.4265}} \\ b = 0.00225 + \frac{772.0074}{1+10^{66.3224(\epsilon_g-0.3987)}} + \frac{0.02404}{1+10^{53.8948(0.5257-\epsilon_g)}} \\ c = 0.1705 - \frac{0.1731}{1+(\epsilon_g/0.5020)^{37.7091}} \end{cases}$	$0.46 \le \epsilon_g < 0.545$
$\begin{cases} a = \left(2124.956 - 2142.3\epsilon_g\right)^{-0.4896} \\ b = \left(0.8223 - 0.1293\epsilon_g\right)^{13.0310} \\ c = \frac{\epsilon_g - 1.0013}{-0.06633+9.1391(\epsilon_g-1.0013)+6.9231(\epsilon_g-1.0013)^2} \end{cases}$	$0.545 \le \epsilon_g < 0.99$
$\begin{cases} a = 0.4243 + \frac{0.8800}{1+exp(-(\epsilon_g-0.9942)/0.00218)}\left(1 - \frac{1}{1+exp(-(\epsilon_g-0.9989)/0.00003)}\right) \\ b = 0.01661 + 0.2436exp\left(-0.5\left(\frac{\epsilon_g-0.9985}{0.00191}\right)^2\right) \\ c = 0.0825 - 0.0574exp\left(-0.5\left(\frac{\epsilon_g-0.9979}{0.00703}\right)^2\right) \end{cases}$	$0.99 \le \epsilon_g < 0.9997$
$\begin{cases} a = 1 \\ c = 0 \end{cases}$	$0.9997 \le \epsilon_g \le 1.0$

region and fall down with a high volume fraction near the wall, are well predicted by the time-averaged and instantaneous simulation results. The solutions of both turbulent fluidized bed and circulating fluidized bed agree well with the experimental measurement. The GKS-UGKWP will become a reliable tool to capture multi-scale flow physics in the fluidized bed simulation with its further development.

Declaration of competing interest

The authors declare that they have no known competing financial interests or personal relationships that could have appeared to influence the work reported in this paper.

Data availability

Data will be made available on request.

Acknowledgments

The current research is supported by National Science Foundation of China (No. 12172316), Hong Kong research grant council (16208021, 16301222), and Department of Science and Technology of Guangdong Province (Grant No. 2020B1212030001).

Appendix. Parameters in EMMS drag model

The specific values of model parameters (a, b, c) to calculate the heterogeneity index H_D in EMMS drag model are listed as below [48,49], see Table 1.

References

[1] Falah Alobaid, Naser Almohammed, Massoud Massoudi Farid, Jan May, Philip Rößger, Andreas Richter, Bernd Epple, Progress in CFD simulations of fluidized beds for chemical and energy process engineering, Prog. Energy Combust. Sci. (2021) 100930.
[2] M.A. van der Hoef, M. van Sint Annaland, N.G. Deen, J.A.M. Kuipers, Numerical simulation of dense gas-solid fluidized beds: A multiscale modeling strategy, Annu. Rev. Fluid Mech. 40 (1) (2008) 47–70.
[3] Wenqi Zhong, Aibing Yu, Guanwen Zhou, Jun Xie, Hao Zhang, CFD simulation of dense particulate reaction system: Approaches, recent advances and applications, Chem. Eng. Sci. 140 (2016) 16–43.
[4] Junwu Wang, Continuum theory for dense gas-solid flow: A state-of-the-art review, Chem. Eng. Sci. (ISSN: 0009-2509) 215 (2020) 115428.
[5] Huilin Lu, Dimitri Gidaspow, Shuyan Wang, Computational Fluid Dynamics and the Theory of Fluidization: Applications of the Kinetic Theory of Granular Flow, Springer Nature, 2021.
[6] C.K.K. Lun, S. Br Savage, D.J. Jeffrey, N. Chepurniy, Kinetic theories for granular flow: Inelastic particles in Couette flow and slightly inelastic particles in a general flowfield, J. Fluid Mech. 140 (1984) 223–256.
[7] Dimitri Gidaspow, Multiphase Flow and Fluidization: Continuum and Kinetic Theory Descriptions, Academic Press, 1994.
[8] Daniele L. Marchisio, Rodney O. Fox, Computational Models for Polydisperse Particulate and Multiphase Systems, Cambridge University Press, 2013.
[9] Jing Wang, Xizhong Chen, Wei Bian, Bidan Zhao, Junwu Wang, Quantifying the non-equilibrium characteristics of heterogeneous gas–solid flow of smooth, inelastic spheres using a computational fluid dynamics–discrete element method, J. Fluid Mech. 866 (2019) 776–790.
[10] Yutaka Tsuji, Toshihiro Kawaguchi, Toshitsugu Tanaka, Discrete particle simulation of two-dimensional fluidized bed, Powder Technol. 77 (1) (1993) 79–87.
[11] Wei Ge, Limin Wang, Ji Xu, Feiguo Chen, Guangzheng Zhou, Liqiang Lu, Qi Chang, Jinghai Li, Discrete simulation of granular and particle-fluid flows: From fundamental study to engineering application, Rev. Chem. Eng. 33 (6) (2017) 551–623.
[12] Mikio Sakai, Minami Abe, Yusuke Shigeto, Shin Mizutani, Hiroyuki Takahashi, Axelle Viré, James R. Percival, Jiansheng Xiang, Christopher C. Pain, Verification and validation of a coarse grain model of the DEM in a bubbling fluidized bed, Chem. Eng. J. 244 (2014) 33–43.
[13] Liqiang Lu, Ji Xu, Wei Ge, Guoxian Gao, Yong Jiang, Mingcan Zhao, Xinhua Liu, Jinghai Li, Computer virtual experiment on fluidized beds using a coarse-grained discrete particle method-EMMS-DPM, Chem. Eng. Sci. 155 (2016) 314–337.
[14] Peter J. O'Rourke, Paul Pinghua Zhao, Dale Snider, A model for collisional exchange in gas/liquid/solid fluidized beds, Chem. Eng. Sci. 64 (8) (2009) 1784–1797.
[15] Dimitri Gidaspow, Veeraya Jiradilok, Computational Techniques: The Multiphase CFD Approach to Fluidization and Green Energy Technologies, Nova Science Publishers, Incorporated, 2010.
[16] Liqiang Lu, Ji Xu, Wei Ge, Yunpeng Yue, Xinhua Liu, Jinghai Li, EMMS-based discrete particle method (EMMS–DPM) for simulation of gas–solid flows, Chem. Eng. Sci. 120 (2014) 67–87.
[17] Qinggong Wang, Yuqing Feng, Junfu Lu, Weidi Yin, Hairui Yang, Peter J. Witt, Man Zhang, Numerical study of particle segregation in a coal beneficiation fluidized bed by a TFM-DEM hybrid model: Influence of coal particle size and density, Chem. Eng. J. 260 (2015) 240–257.
[18] Xizhong Chen, Junwu Wang, Jinghai Li, Multiscale modeling of rapid granular flow with a hybrid discrete-continuum method, Powder Technol. 304 (2016) 177–185.
[19] Niels G. Deen, EA.J.F. Peters, Johan T. Padding, JAM Kuipers, Review of direct numerical simulation of fluid–particle mass, momentum and heat transfer in dense gas–solid flows, Chem. Eng. Sci. 116 (2014) 710–724.
[20] Liqiang Lu, Xiaowen Liu, Tingwen Li, Limin Wang, Wei Ge, Sofiane Benyahia, Assessing the capability of continuum and discrete particle methods to simulate gas-solids flow using DNS predictions as a benchmark, Powder Technol. 321 (2017) 301–309.
[21] Kun Luo, Zhuo Wang, Junhua Tan, Jianren Fan, An improved direct-forcing immersed boundary method with inward retraction of Lagrangian points for simulation of particle-laden flows, J. Comput. Phys. 376 (2019) 210–227.
[22] Bo Kong, Rodney O. Fox, A solution algorithm for fluid–particle flows across all flow regimes, J. Comput. Phys. 344 (2017) 575–594.
[23] Aaron S. Baumgarten, Ken Kamrin, A general fluid-sediment mixture model and constitutive theory validated in many flow regimes, J. Fluid Mech. 861 (2019) 721–764.
[24] Xiaojian Yang, Chang Liu, Xing Ji, Wei Shyy, Kun Xu, Unified gas-kinetic wave-particle methods VI: Disperse dilute gas-particle multiphase flow, Commun. Comput. Phys. 31 (3) (2022) 669.

[25] Xiaojian Yang, Wei Shyy, Kun Xu, Unified gas-kinetic wave–particle method for gas–particle two-phase flow from dilute to dense solid particle limit, Phys. Fluids 34 (2) (2022) 023312.
[26] Kun Xu, Juan-Chen Huang, A unified gas-kinetic scheme for continuum and rarefied flows, J. Comput. Phys. 229 (20) (2010) 7747–7764.
[27] Kun Xu, Direct Modeling for Computational Fluid Dynamics: Construction and Application of Unified Gas-Kinetic Schemes, Vol. 4, World Scientific, 2014.
[28] Kun Xu, A Unified Computational Fluid Dynamics Framework from Rarefied to Continuum Regimes, Elements in Aerospace Engineering, Cambidge University Press, 2021.
[29] Wenjun Sun, Song Jiang, Kun Xu, An asymptotic preserving unified gas kinetic scheme for gray radiative transfer equations, J. Comput. Phys. 285 (2015) 265–279.
[30] Chang Liu, Zhao Wang, Kun Xu, A unified gas-kinetic scheme for continuum and rarefied flows VI: Dilute disperse gas-particle multiphase system, J. Comput. Phys. 386 (2019) 264–295.
[31] Chang Liu, Yajun Zhu, Kun Xu, Unified gas-kinetic wave-particle methods I: Continuum and rarefied gas flow, J. Comput. Phys. 401 (2020) 108977.
[32] Yajun Zhu, Chang Liu, Chengwen Zhong, Kun Xu, Unified gas-kinetic wave-particle methods II. Multiscale simulation on unstructured mesh, Phys. Fluids 31 (6) (2019) 067105.
[33] Chang Liu, Kun Xu, Unified gas-kinetic wave-particle methods IV: Multi-species gas mixture and plasma transport, Adv. Aerodynam. 3 (1) (2021) 1–31.
[34] Xiaocong Xu, Yipei Chen, Kun Xu, Modeling and computation for non-equilibrium gas dynamics: Beyond single relaxation time kinetic models, Phys. Fluids 33 (1) (2021) 011703.
[35] Kun Xu, A gas-kinetic BGK scheme for the Navier–Stokes equations and its connection with artificial dissipation and Godunov method, J. Comput. Phys. 171 (1) (2001) 289–335.
[36] Fengxiang Zhao, Xing Ji, Wei Shyy, Kun Xu, An acoustic and shock wave capturing compact high-order gas-kinetic scheme with spectral-like resolution, J. Comput. Phys. 449 (2022) 110812.
[37] Guiyu Cao, Hongmin Su, Jinxiu Xu, Kun Xu, Implicit high-order gas kinetic scheme for turbulence simulation, Aerosp. Sci. Technol. 92 (2019) 958–971.
[38] Xing Ji, Fengxiang Zhao, Wei Shyy, Kun Xu, A HWENO reconstruction based high-order compact gas-kinetic scheme on unstructured mesh, J. Comput. Phys. 410 (2020) 109367.
[39] Xiaojian Yang, Xing Ji, Wei Shyy, Kun Xu, Comparison of the performance of high-order schemes based on the gas-kinetic and HLLC fluxes, J. Comput. Phys. 448 (2022) 110706.
[40] Xi Gao, Cheng Wu, You-wei Cheng, Li-jun Wang, Xi Li, Experimental and numerical investigation of solid behavior in a gas-solid turbulent fluidized bed, Powder Technol. 228 (2012) 1–13.
[41] Jun Xie, Wenqi Zhong, Aibing Yu, MP-PIC modeling of CFB risers with homogeneous and heterogeneous drag models, Adv. Powder Technol. 29 (11) (2018) 2859–2871.
[42] Duan Z. Zhang, W. Brian VanderHeyden, The effects of mesoscale structures on the macroscopic momentum equations for two-phase flows, Int. J. Multiph. Flow. 28 (5) (2002) 805–822.
[43] Tim Mckeen, Todd Pugsley, Simulation and experimental validation of a freely bubbling bed of FCC catalyst, Powder Technol. 129 (1–3) (2003) 139–152.
[44] Jinghai Li, Mooson Kwauk, Particle-Fluid Two-Phase Flow: The Energy-Minimization Multi-Scale Method, Metallurgical Industry Press, 1994.
[45] Ning Yang, Wei Wang, Wei Ge, Jinghai Li, CFD simulation of concurrent-up gas-solid flow in circulating fluidized beds with structure-dependent drag coefficient, Chem. Eng. J. 96 (1–3) (2003) 71–80.
[46] Ning Yang, Wei Wang, Wei Ge, Linna Wang, Jinghai Li, Simulation of heterogeneous structure in a circulating fluidized-bed riser by combining the two-fluid model with the EMMS approach, Ind. Eng. Chem. Res. 43 (18) (2004) 5548–5561.
[47] Wei Wang, Jinghai Li, Simulation of gas–solid two-phase flow by a multi-scale CFD approach—of the EMMS model to the sub-grid level, Chem. Eng. Sci. 62 (1–2) (2007) 208–231.
[48] Bona Lu, Wei Wang, Jinghai Li, Eulerian simulation of gas–solid flows with particles of Geldart groups A, B and D using EMMS-based meso-scale model, Chem. Eng. Sci. 66 (20) (2011) 4624–4635.
[49] Fei Li, Feifei Song, Sofiane Benyahia, Wei Wang, Jinghai Li, MP-PIC simulation of CFB riser with EMMS-based drag model, Chem. Eng. Sci. 82 (2012) 104–113.
[50] Masayuki Horio, Kenji Morishita, Osamu Tachibana, Naoki Murata, Solid distribution and movement in circulating fluidized beds, in: Circulating Fluidized Bed Technology, Elsevier, 1988, pp. 147–154.
[51] A. Passalacqua, R.O. Fox, R. Garg, S. Subramaniam, A fully coupled quadrature-based moment method for dilute to moderately dilute fluid–particle flows, Chem. Eng. Sci. 65 (7) (2010) 2267–2283.
[52] Sydney Chapman, Thomas George Cowling, The Mathematical Theory of Non-Uniform Gases: An Account of the Kinetic Theory of Viscosity, Thermal Conduction and Diffusion in Gases, Cambridge University Press, 1970.
[53] Simon Schneiderbauer, Andreas Aigner, Stefan Pirker, A comprehensive frictional-kinetic model for gas–particle flows: Analysis of fluidized and moving bed regimes, Chem. Eng. Sci. 80 (2012) 279–292.
[54] Sebastian Chialvo, Sankaran Sundaresan, A modified kinetic theory for frictional granular flows in dense and dilute regimes, Phys. Fluids 25 (7) (2013) 070603.
[55] Junnan Zhao, Guodong Liu, Wei Li, Xiaolong Yin, Yao Wu, Chunlei Wang, Huilin Lu, A comprehensive stress model for gas-particle flows in dense and dilute regimes, Chem. Eng. Sci. 226 (2020) 115833.
[56] Paul C. Johnson, Roy Jackson, Frictional-collisional constitutive relations for granular materials, with application to plane shearing, J. Fluid Mech. 176 (1987) 67–93.
[57] Anuj Srivastava, Sankaran Sundaresan, Analysis of a frictional-kinetic model for gas-particle flow, Powder Technol. 129 (1–3) (2003) 72–85.
[58] Ryan W. Houim, Elaine S. Oran, A multiphase model for compressible granular-gaseous flows: Formulation and initial tests, J. Fluid Mech. 789 (2016) 166.
[59] Mamoru Ishii, Takashi Hibiki, Thermo-Fluid Dynamics of Two-Phase Flow, Springer Science & Business Media, 2006.
[60] Eleuterio F. Toro, Riemann Solvers and Numerical Methods for Fluid Dynamics: A Practical Introduction, Springer Science & Business Media, 2013.
[61] Kun Hong, Sheng Chen, Wei Wang, Jinghai Li, Fine-grid two-fluid modeling of fluidization of Geldart a particles, Powder Technol. 296 (2016) 2–16.
[62] David Pallarès, Filip Johnsson, Macroscopic modelling of fluid dynamics in large-scale circulating fluidized beds, Prog. Energy Combust. Sci. 32 (5–6) (2006) 539–569.